

Resonant two-magnon Raman scattering in parent compounds of high- T_c superconductors.

Andrey V. Chubukov

Department of Physics, University of Wisconsin-Madison, 1150 University ave., Madison, WI 53706

and P.L. Kapitza Institute for Physical Problems, Moscow, Russia

David M. Frenkel

Texas Center for Superconductivity, University of Houston, Houston, TX 77204-5932*

and Department of Physics, Science and Technology Center for Superconductivity, University of Illinois at Urbana-Champaign, 1110 West Green Street, Urbana, IL 61801

(today)

Abstract

We propose a theory of two-magnon Raman scattering from the insulating parent compounds of high- T_c superconductors, which contains information not only on magnetism, but also on the electronic properties in these materials. We use spin density wave formalism for the Hubbard model, and study diagrammatically the profile of the two-magnon scattering and its intensity dependence on the incoming photon frequency ω_i both for $\omega_i \ll U$ and in the resonant regime, in which the energy of the incident photon is close to the gap between conduction and valence bands. In the nonresonant case, we identify the diagrams which contribute to the conventional Loudon-Fleury Hamiltonian. In the resonant regime, where most of the experiments have been done, we find that the dominant contribution to Raman intensity comes from a different diagram, one which allows for a simultaneous vanishing of all three of

its denominators (i.e., a triple resonance). We study this diagram in detail and show that the triple resonance, combined with the spin-density-wave dispersion relation for the carriers, explains the unusual features found in the two-magnon profile and in the two-magnon peak intensity dependence on the incoming photon frequency. In particular, our theory predicts a maximum of the two-magnon peak intensity right at the upper edge of the features in the optical data, which has been one of the key experimental puzzles.

I. INTRODUCTION

There is a widespread belief that strong electron-electron correlations in the high- T_c compounds may hold a clue to the phenomenon of high-temperature superconductivity.¹⁻³ One of the manifestations of these correlations is in the fact that the insulating parent compounds are antiferromagnets. An important probe of antiferromagnetism is magnetic Raman scattering.⁴⁻⁷ Its prominent signature in the underdoped high- T_c materials is a two-magnon peak observed at about 3000 cm^{-1} . To first approximation, this peak can be attributed to inelastic scattering from the two-magnon excitations.⁸ In fact, Raman experiments yielded the first estimate of the exchange interaction constant in La_2CuO_4 .⁸⁻¹¹ The two-magnon peak has also been observed in the electron-doped materials¹² and more recently¹³ in the underdoped $YBa_2Cu_3O_{6+x}$ materials (up to $x = 0.9$).

The traditional framework for understanding the two-magnon Raman scattering in antiferromagnets has been an effective Hamiltonian for the interaction of light with spin degrees of freedom known as the Loudon-Fleury Hamiltonian¹⁴

$$H = \alpha \sum_{\langle ij \rangle} (\hat{\mathbf{e}}_i \cdot \mathbf{R}_{ij})(\hat{\mathbf{e}}_f \cdot \mathbf{R}_{ij}) \mathbf{S}_i \cdot \mathbf{S}_j. \quad (1)$$

Here $\hat{\mathbf{e}}_i$ and $\hat{\mathbf{e}}_f$ are the polarization vectors of the in- and outgoing photons, α is the (generally poorly known) coupling constant, and \mathbf{R}_{ij} is a vector along the bond connecting two nearest neighbor sites i and j . This equation has been reexamined in recent years to better account for a possible importance of quantum fluctuations, the four-magnon processes, and the further neighbor terms.^{6,15,16}

The Loudon-Fleury theory is expected to work well when the frequencies of the incoming and outgoing photons are considerably smaller than the gap between conduction and valence bands. The experimental reality in high- T_c materials is such, however, that the two-magnon scattering is observed mostly in or near the so-called resonant regime, when the frequencies of the ingoing and/or outgoing photons are close to the gap value. This is simply a consequence of the fact that the experiments are mostly done with the visible or near ultraviolet lasers,

while the gap and the upper Hubbard band states lie in the same range of frequencies (roughly between 2 eV and 3 eV) in the high- T_c materials. The experimental cross-sections vary strongly in this range of incident photon frequencies,^{10,17,18} and it becomes an issue whether the Loudon-Fleury Hamiltonian is still applicable. Whatever the answer to this question, we still need to have the means of evaluating the variation of the overall scale of the coupling constant α in Eq. (1) with the incident photon frequency ω_i .

The profile of the Raman cross-section as a function of the *transferred* photon frequency is shown in Fig. 1. The two-magnon peak is clearly identifiable. The behavior of the two-magnon peak height as a function of the *incident* photon frequency is presented in Fig. 2, where the absorptive part of the dielectric constant is also shown for comparison.

The key experimental features that require explanation are the following:

In Fig. 1:

- (a) *Asymmetry of the two-magnon peak profile*: the two-magnon peak is asymmetric, with the spectral weight shifted to higher frequencies.
- (b) *Selection rules*: Loudon-Fleury Hamiltonian predicts no scattering in the A_{1g} configuration; experimentally in the resonant regime the A_{1g} cross-section is about half of that in the B_{1g} geometry.
- (c) *Stability of the two-magnon peak profile*: as the incident photon frequency changes over the frequency range from 15,000 to 22,000 cm^{-1} , the two-magnon scattering intensity profile merely scales with incident frequency, without a noticeable change in shape. (However, at higher photon energies, a distortion of the Raman spectrum occurs.)

In Fig. 2:

- (a) *A single peak*: ordinarily one might expect two peaks, the so called ingoing and outgoing resonances,^{19,20} and here only one is observed.
- (b) *Peak location*: a comparison with the dielectric constant shows that the strength of the two-magnon Raman scattering is at its maximum away from the band edge, in fact right at the upper end of the features in the optical data that can be interpreted as the particle-hole excitations between the lower and upper Hubbard bands. (Phonons, on the contrary, are

known to resonate with the features in the dielectric constant.²¹⁾

Raman scattering in a one-band model of correlated electrons has been considered several times in the literature.^{16,22,23} Shastry and Shraiman²² have recently given a derivation of the Loudon-Fleury Hamiltonian starting from the usual large- U Hubbard model. Working in a localized basis, they performed a hopping expansion controlled by $t/(U - \omega)$, where t and U are the nearest-neighbor hopping and on-site Coulomb repulsion, and ω is of the order of the photon frequencies. The leading term in the expansion turned out to be the Loudon-Fleury Hamiltonian, Eq. (1).

A simple, though somewhat crude interpretation of this outcome is to envision spins in a classical Neel state. The incoming photon is absorbed by moving, say, a down spin to the neighboring site occupied by an up spin. The up spin then returns to the formerly down site, emitting the outgoing photon. The overall result is light scattering accompanied by the nearest neighbor spin exchange, which is encoded in Eq. (1). This process is shown in Fig. 3.

Notice that the intermediate state in this process has a doubly occupied site, and is thus of order U above the ground state in energy. When the photon energy is far smaller than U , no further precision in specifying the intermediate state's energy is needed, and the leading order term is sufficient. When $(U - \omega)$ becomes of order t (resonant regime), all of the terms in the expansion in $t/(U - \omega)$ are of the same order, and the leading term can no longer provide a solution. However, it is in this regime that the cross-sections sensitively depend not just on the magnetic, but also on the carrier properties, and this makes it a especially important to the field of high- T_c superconductivity.

We will discuss the form of the Raman vertex in both the nonresonant and resonant regimes later in the paper and here merely note that, on physical grounds, the multiple hops affect the single-particle Green's function in two distinct ways. First, the multiple hops is a way to generate the band structures of the doubly occupied sites and holes, i.e., they produce a dispersion in the coherent part of the single-particle Green's function. Second, they produce a distortion of the spin background around each hole which gives rise to the

incoherent part of the Green's function. Since resonance is a phenomenon contingent upon the vanishing of the denominators in perturbation theory, it is plausible to assume that the incoherent parts of the Green's functions are of lesser importance. We thus model our particle and hole Green's functions as fully coherent, but having a certain dispersion, which at half-filling we take to be that of the spin density wave (SDW) solution of the Hubbard model.²⁵ We regard our ability to address the experimental results on the basis of this dispersion relation as partial evidence of the validity of the SDW picture not only for the antiferromagnetism, but also for the hole dynamics.

We wish to stress that this is not a trivial distinction. There have been many interesting theoretical studies of the single hole problem in the Hubbard and the t-J models.^{25–30} However, even such a basic feature as the band structure of a single hole has not been experimentally tested. Indeed, in the low-doping regime the holes are trapped near the dopant sites. Even in the translationally invariant case, the phonon polaron effects^{31,32} could still destroy the hole dispersion predicted on the basis of purely electronic models. Resonant Raman scattering right at half-filling is sensitive to the details of the dispersion of the fermionic quasiparticles and thus provides an experimental information about the single hole dispersion without having to dope the material.

Before proceeding to the description of our calculations, we would like to make two comments about the model we use. First, in this paper we exclusively consider the one-band Hubbard model. This by itself is a simplification, since in the “first-principles” calculation one would start with a three-band model for the CuO_2 unit. Within this model, the lowest gap (about $2 eV$) is a charge-transfer gap between Cu and O bands.³³ However, it is generally accepted that at energies comparable to this gap the hybridization between Cu and O orbitals is relevant, and one can effectively describe the system by a single degree of freedom per CuO_2 unit, which in turn implies that the three-band Hubbard model can be reduced to an effective one-band Hubbard model.^{34–36} The relevant parameter which allows the reduction in the number of degrees of freedom is the splitting of the triplet and singlet states of the O and Cu spins in the Zhang-Rice theory.³⁴ Their estimate of this splitting is several

electron volts, and thus the singlet states relevant to our analysis are well-separated from the triplet states. This is corroborated by the measured behavior of the dielectric constant. For example, in GdCuO_2 there are strong absorption features in the imaginary part of the dielectric constant around $1.7 - 2.7 \text{ eV}$ and around 5 eV , but only a featureless continuum in between.³⁷ We therefore expect that the one-band Hubbard model already captures all the essential physics of Raman scattering up to photon energies of order $3 - 4 \text{ eV}$.

Our second comment concerns the hopping term in the Hamiltonian. In this paper, we restrict our model to contain only the nearest-neighbor hopping, t . Meanwhile, it was suggested³⁸ on the basis of the photoemission data for YBaCuO_7 , that the next-nearest-neighbor hopping term in the 123 compounds is rather large, $t' \sim -0.5t$. For La -based compounds, t' was estimated³⁶ to be $t' \sim -0.2t$. At finite doping, the restriction to only the t term requires care, as the spin-density wave theory (which we will use in most of our considerations) is meaningless near the minima of the quasiparticle band, unless one takes into account the self-energy corrections which lift the degeneracy of the quasiparticle spectrum along the reduced Brillouin zone boundary.^{39,40} Fortunately, as we will see below, the two-magnon Raman scattering in cuprates is not a phenomenon that is associated with the minima of the quasiparticle band, and therefore the details of the quasiparticle dispersion right near those minima will not be important in our analysis. For this reason, we believe that for a qualitative analysis of Raman scattering in cuprates, one can use the simplest model with just the nearest-neighbor hopping.

The paper is organized as follows. Sec. II discusses the general formalism of the two-magnon Raman scattering in antiferromagnetic insulators. In Sec. III, we consider the nonresonant scattering. In particular, we show how the results of Shastry and Shraiman are reproduced in the SDW formalism. We will also discuss the location and shape of the two-magnon peak. Sec. IV is the main part of the paper. We argue that the phenomenon of multiple resonance, described in detail in that section, is a way to explain the unusual features in Figs. 1 and 2. We study the singularities of the integrals corresponding to that type of resonant behavior, and present the relevant calculations. Finally, in Sec. V,

we present a comparison with the experimental results and state our conclusions. Some technical details of our calculations are contained in the Appendix. Some of the results of this work have been already presented in a short paper.⁴¹

II. GENERAL CONSIDERATIONS

We start with the general theory of magnetic Raman scattering in the Hubbard model. The one-band Hubbard Hamiltonian is

$$H = -t \sum_{\langle i,j \rangle} (c_{i,\sigma}^\dagger c_{j,\sigma} + h.c.) + U \sum_i n_{i\uparrow} n_{i\downarrow}. \quad (2)$$

A straightforward procedure to derive the coupling of light to the fermions in this model was recently described by Shastry and Shraiman.²² In the presence of the slowly varying vector potential $\mathbf{A}(\mathbf{x}, t)$, each fermion operator acquires a phase $e^{(ie/\hbar c) \int \mathbf{A} \cdot d\mathbf{l}}$, and the hopping term gets transformed into

$$H_t = -t \sum_{\langle i,j \rangle} e^{i \frac{e}{\hbar c} \int_i^j \mathbf{A} \cdot d\mathbf{l}} c_{i,\sigma}^\dagger c_{j,\sigma} + h.c. \quad (3)$$

The vector potential is supposed to vary slowly on lattice scales, and one can then approximate the phase factor by

$$\int_i^j \mathbf{A}(\mathbf{l}) \cdot d\mathbf{l} \approx \mathbf{A} \left(\frac{i+j}{2} \right) \cdot \mathbf{R}_{ij}. \quad (4)$$

Substituting this into the expression for H_t and expanding in powers of the vector potential, one obtains upon transforming to the momentum space

$$H_t = H_t^{\mathbf{A}=0} - \frac{e}{\hbar c} \sum_q \mathbf{j}_q \cdot \mathbf{A}_{-q} + \frac{1}{2} \left(\frac{e}{\hbar c} \right)^2 \sum_{q_1} \sum_{q_2} \mathbf{A}_{-q_1} \cdot \tau_{q_1+q_2} \cdot \mathbf{A}_{-q_2}, \quad (5)$$

where the current and the stress-tensor operators are

$$\begin{aligned} j_q^\alpha &= \sum_k \frac{\partial \epsilon_k}{\partial k_\alpha} c_{k+q/2,\sigma}^\dagger c_{k-q/2,\sigma}, \\ \tau_q^{\alpha,\beta} &= \sum_k \frac{\partial^2 \epsilon_k}{\partial k_\alpha \partial k_\beta} c_{k+q/2,\sigma}^\dagger c_{k-q/2,\sigma}, \end{aligned} \quad (6)$$

and ϵ_k is the electron dispersion,

$$\epsilon_k = -2t(\cos k_x + \cos k_y). \quad (7)$$

The vector potential can be quantized in the usual way

$$\mathbf{A}_{q,\lambda} = g_q(\hat{\mathbf{e}}_\lambda l_{-q} + \hat{\mathbf{e}}_\lambda^* l_q^\dagger), \quad (8)$$

where $g_q = (2\pi\hbar c^2/(\omega_q V))^{1/2}$ and ω_q is the light frequency. The velocity of light is several orders of magnitude larger than the Fermi velocity, and therefore we can safely set the momenta of photons equal to zero.

Consider now separately the last two terms in Eq. (5), which contain the vector potential. The last term is already quadratic in \mathbf{A} , so for photon scattering we have to consider only the first-order contribution from it. This contribution does not lead to resonant scattering and, at least in the resonant regime, can be neglected compared to the resonant scattering from the first term. For this reason we neglect the last term in Eq. (5) in this paper, and focus only on the first term which leads to photon scattering in the second order of perturbation theory. This second-order scattering process involves an intermediate particle-hole state of the fermionic system which can emit or absorb collective bosonic excitations before collapsing into the outgoing photon. In particular, in the two-magnon resonant scattering, a photon with the energy ω_i is injected into the antiferromagnetically ordered set of electrons. This photon creates a virtual particle-hole pair which then emits two spin-waves with momenta \mathbf{k} and $-\mathbf{k}$, and then annihilates into an outgoing photon with the energy ω_f .

Ignoring the polaritonic effects, the Raman scattering cross section⁴² is obtained from the lowest-order Golden Rule

$$R = \frac{8\pi^3 e^4}{\hbar^3 V^2 \omega_i \omega_f} \sum_{i,f} |\langle f | M_R | i \rangle|^2 \delta(\hbar\omega_i - \hbar\omega_f + \epsilon_i - \epsilon_f), \quad (9)$$

where ϵ_i and ϵ_f are the energies of the initial and final states of the system ($\epsilon_f - \epsilon_i = \Omega$ is a total frequency of two magnons in the final state), and the summation over the final states f includes the integration over the photon momenta. Further, $\langle f | M_R | i \rangle$ is a matrix element, given by

$$M_R \equiv \langle f | M_R | i \rangle = \sum_n \left[\frac{\langle f | \mathbf{j}_{k_f} \cdot \hat{\mathbf{e}}_f^* | n \rangle \langle n | \mathbf{j}_{-k_i} \cdot \hat{\mathbf{e}}_i | i \rangle}{\epsilon_i + \hbar\omega_i - \epsilon_n + i\delta} + \frac{\langle f | \mathbf{j}_{-k_i} \cdot \hat{\mathbf{e}}_i | n \rangle \langle n | \mathbf{j}_{k_f} \cdot \hat{\mathbf{e}}_f^* | i \rangle}{\epsilon_i - \epsilon_n - \hbar\omega_f + i\delta} \right]. \quad (10)$$

Here the summation is over the intermediate electronic states, labeled as n . Our primary goal will be to calculate the dependence of this matrix element on the incident photon frequency.

For completeness, we also list a number of possible experimental scattering geometries.²² They differ in the polarizations of the incident ($\hat{\mathbf{e}}_i$) and scattered ($\hat{\mathbf{e}}_f$) photons. For the linearly polarized light, the scattering geometries are

$$\begin{aligned} A_{1g} : \hat{\mathbf{e}}_i &= \frac{\hat{\mathbf{x}} + \hat{\mathbf{y}}}{\sqrt{2}}, \quad \hat{\mathbf{e}}_f = \frac{\hat{\mathbf{x}} + \hat{\mathbf{y}}}{\sqrt{2}}; \\ B_{1g} : \hat{\mathbf{e}}_i &= \frac{\hat{\mathbf{x}} + \hat{\mathbf{y}}}{\sqrt{2}}, \quad \hat{\mathbf{e}}_f = \frac{\hat{\mathbf{x}} - \hat{\mathbf{y}}}{\sqrt{2}}; \\ B_{2g} : \hat{\mathbf{e}}_i &= \hat{\mathbf{x}}, \quad \hat{\mathbf{e}}_f = \hat{\mathbf{y}}. \end{aligned} \quad (11)$$

For the circularly polarized light, the scattering geometries are

$$\begin{aligned} LL : \hat{\mathbf{e}}_i &= \frac{\hat{\mathbf{x}} + i\hat{\mathbf{y}}}{\sqrt{2}}, \quad \hat{\mathbf{e}}_f = \frac{\hat{\mathbf{x}} + i\hat{\mathbf{y}}}{\sqrt{2}}; \\ LR : \hat{\mathbf{e}}_i &= \frac{\hat{\mathbf{x}} + i\hat{\mathbf{y}}}{\sqrt{2}}, \quad \hat{\mathbf{e}}_f = \frac{\hat{\mathbf{x}} - i\hat{\mathbf{y}}}{\sqrt{2}}. \end{aligned} \quad (12)$$

The scattering in each geometry measures a particular combination of the components of the scattering tensor. It is convenient to decompose $\langle f | M_R | i \rangle$ into four one-dimensional representations of the 2D square lattice symmetry group D_{4h} :

$$\begin{aligned} M_R^{A_1} &= \langle x | M_R | x \rangle + \langle y | M_R | y \rangle, \\ M_R^{A_2} &= \langle x | M_R | y \rangle - \langle y | M_R | x \rangle, \\ M_R^{B_1} &= \langle x | M_R | x \rangle - \langle y | M_R | y \rangle, \\ M_R^{B_2} &= \langle x | M_R | y \rangle + \langle y | M_R | x \rangle. \end{aligned} \quad (13)$$

Then, the scattering in the experimental A_{1g} geometry measures a combination of $M_R^{A_1}$ and $M_R^{B_2}$, the scattering in the B_{1g} geometry measures a combination of $M_R^{B_1}$ and $M_R^{A_2}$, etc. In

the two-magnon Raman scattering, the energy transfer $\omega_i - \omega_f$ is small compared to the gap between conduction and valence bands. In this situation, the dominant components of the scattering tensor are found experimentally to be those of $M_R^{A_1}$ and $M_R^{B_1}$ symmetry.¹³ It is therefore sufficient to study scattering in the A_{1g} and B_{1g} experimental geometries.

The states in the general expression of Eq. (10) for the matrix element are the full many-body states of the system, which contain both the electronic and spin excitations. Therefore, to fully describe the two-magnon Raman scattering we will need two different types of vertices. The first is the interaction between the vector potential of light and the fermionic current density – this vertex is given in Eq. (5). The second is the interaction between the fermions and the spin-waves.

A convenient way to express both types of vertices on equal footing is to use the spin density wave (SDW) formalism²⁵ to describe the electronic state at half-filling and the excitations around it. In the SDW formalism, one introduces a long-range order in $\mathbf{S}_q = \sum_k c_{k+q,\alpha}^\dagger \sigma_{\alpha,\beta} c_{k,\beta}$ with $\mathbf{q} = \mathbf{Q} \equiv (\pi, \pi)$ and uses it to decouple the Hubbard interaction term. The diagonalization then yields two bands of electronic states (the conduction and valence bands) with the gap $2\Delta \sim U$ in the strong coupling limit that will be assumed throughout this work.

In terms of the conduction and valence band quasiparticle operators $a_{k\sigma}^\dagger$ and $b_{k\sigma}^\dagger$, the quadratic part of the Hubbard Hamiltonian takes the form

$$H = \sum'_{k\sigma} E_k (a_{k\sigma}^\dagger a_{k\sigma} - b_{k\sigma}^\dagger b_{k\sigma}), \quad (14)$$

where the prime restricts summation to the magnetic Brillouine zone, and the quasiparticle energy is $E_k = \sqrt{\epsilon_k^2 + \Delta^2}$. We will also need the relation between the new and the old quasiparticle operators. It reads

$$\begin{aligned} c_{k,\sigma} &= u_k a_{k,\sigma} + v_k b_{k,\sigma}, \\ c_{k+Q,\sigma} &= \text{sgn}(\sigma)(u_k b_{k,\sigma} - v_k a_{k,\sigma}), \end{aligned} \quad (15)$$

where the fermionic Bogolyubov coefficients are

$$u_k = \sqrt{\frac{1}{2} \left(1 + \frac{\epsilon_k}{E_k}\right)}, \quad v_k = \sqrt{\frac{1}{2} \left(1 - \frac{\epsilon_k}{E_k}\right)}. \quad (16)$$

Note that in the large- U limit, $2u_k v_k \simeq 1$.

We now discuss the vertices. The current operator can be rewritten as

$$\mathbf{j}_{q=0} = \sum_k \frac{\partial \epsilon_k}{\partial \mathbf{k}} c_{k\sigma}^\dagger c_{k\sigma} = \sum_k' \frac{\partial \epsilon_k}{\partial \mathbf{k}} (c_{k\sigma}^\dagger c_{k\sigma} - c_{k+Q,\sigma}^\dagger c_{k+Q,\sigma}). \quad (17)$$

Upon performing the Bogolyubov transformation, we obtain the current in terms of valence and conduction band fermions,

$$\begin{aligned} \mathbf{j}_{q=0} = \sum_{k\sigma}' \frac{\partial \epsilon_k}{\partial \mathbf{k}} & \left[(2u_k v_k) (a_{k\sigma}^\dagger b_{k\sigma} + b_{k\sigma}^\dagger a_{k\sigma}) \right. \\ & \left. + (u_k^2 - v_k^2) (a_{k\sigma}^\dagger a_{k\sigma} - b_{k\sigma}^\dagger b_{k\sigma}) \right]. \end{aligned} \quad (18)$$

Note that the terms with only valence or conduction fermions have a smallness in t/U from the Bogolyubov coefficients. Keeping only the leading terms, we obtain

$$\mathbf{j}_{q=0} \Rightarrow \sum_{k\sigma}' \frac{\partial \epsilon_k}{\partial \mathbf{k}} (a_{k\sigma}^\dagger b_{k\sigma} + b_{k\sigma}^\dagger a_{k\sigma}), \quad (19)$$

which is the expression we use almost exclusively in this paper.

We can now obtain an expression for the optical conductivity $\sigma(\mathbf{q} = \mathbf{0}, \omega)$ in the SDW state. From Kubo formula, in terms of the particle current given above,

$$\sigma(\omega) = e^2 \frac{\pi}{\omega} \sum_n \delta(\epsilon_n - \epsilon_0 - \omega) |\langle n | j_x(\mathbf{q} = \mathbf{0}) | 0 \rangle|^2, \quad (20)$$

where $\epsilon_n - \epsilon_0$ is the excitation energy between the ground and excited SDW states. At half-filling, we only have to retain the intraband terms in Eq. (18), and, using also Eq. (14) for the valence and conduction fermion energies, we obtain

$$\sigma(\omega) = e^2 \frac{4t^2 \pi}{\omega} \sum_{k\sigma}' \sin^2 k_x \frac{\Delta^2}{E_k^2} \delta(\omega - 2E_k), \quad (21)$$

which agrees with the result in Ref. 24. We have obtained a compact closed form answer for $\sigma(\omega)$ in terms of complete elliptic integrals. The answer is nonzero when the photon energy is within the bands,

$$\sigma(\lambda) = \frac{e^2}{4\pi\hbar} \left(\frac{2\Delta}{\omega}\right)^2 \left[\frac{4}{\sqrt{\lambda}} E \left(\sqrt{1 - \frac{\lambda}{4}} \right) - \sqrt{\lambda} K \left(\sqrt{1 - \frac{\lambda}{4}} \right) \right], \quad 0 < \lambda < 4, \quad (22)$$

where $\lambda = (\omega^2 - (2\Delta)^2)/16t^2$ counts the photon energy from the optical gap edge, and we momentarily restore \hbar for reference purposes. When $t/U \ll 1$, $2\Delta/\omega \approx 1$, and $\lambda \approx (\omega - U)U/8t^2$. The plot of $\sigma(\omega)$ at $t \ll U$ is given below in Fig. 11(a). It has a square root singularity at $\lambda = 0^+$ and vanishes as $\lambda \rightarrow 4^-$. The singularity at $\lambda = 0^+$ is due to the degeneracy of the mean-field dispersion E_k along the reduced Brillouine zone boundary. As we described above, this singularity is an artifact of mean-field SDW approach. When the degeneracy in E_k is broken by either quantum fluctuations or hopping to further neighbors, only the more usual logarithmic singularity will survive at $\omega = 2\Delta$. On the other hand, the vanishing of $\sigma(\omega)$ at $\lambda = 4$ is due to the vanishing of the current form-factor $\sin k_x$ in Eq. (21) at $\mathbf{k} = \mathbf{0}$, which is where the *maximum* optical gap occurs for SDW states. There is no mean-field degeneracy at $\mathbf{k} = \mathbf{0}$, and thus $\sigma = 0$ at the top of the fermionic band should survive also beyond the mean-field approximation.

The remaining ingredients for Raman scattering are the magnon propagator and the magnon-fermion scattering vertex. In the SDW formalism the magnons are described as collective modes in the transverse spin channel.²⁵ Specifically, the spin-wave excitations correspond to the poles of the transverse spin susceptibility

$$\chi^{+-}(q, q'; t) = i \langle T (S_q^+(t) S_{-q'}^-(0)) \rangle. \quad (23)$$

The total transverse susceptibility is given in the SDW theory by the diagrams containing a sequence of bubbles made of the conduction and valence fermions with the four-fermion vertices connecting them. The restriction to only such diagrams can be justified if one extends the original $S = 1/2$ Hubbard model to large S by considering $2S$ orbitals at a given site.⁴³ At half-filling this extension transforms the Hubbard interaction term into the Hund's rule coupling which favors the maximum possible spin S at each site. Notice that in this situation the mean-field gap between lower and upper Hubbard bands is related to U as $2\Delta = 2US$. In relating the large- S calculations to the $S = 1/2$ case, it is the gap Δ

which should be kept fixed.

The SDW spin susceptibility has been considered several times in the literature.^{25,39,44} Since the unit cell is doubled due to the presense of the antiferromagnetic long range order, we have two susceptibilities — one with zero transferred momentum, and one with the momentum transfer $\mathbf{Q} = (\pi, \pi)$. The explicit forms of these susceptibilities are

$$\begin{aligned}\chi^\pm(q, q, \omega) &= -S \sqrt{\frac{1-\gamma_q}{1+\gamma_q}} \left[\frac{1}{\omega - \Omega_q + i\delta} - \frac{1}{\omega + \Omega_q - i\delta} \right], \\ \chi^\pm(q, q + Q, \omega) &= -S \left[\frac{1}{\omega - \Omega_q + i\delta} + \frac{1}{\omega + \Omega_q - i\delta} \right].\end{aligned}\quad (24)$$

Here $\Omega_q = 4JS\sqrt{1-\gamma_q^2}$ is the magnon frequency, and $J = 4t^2/(2S)^2U$ is the exchange integral.

Further, a sequence of bubble diagrams can be viewed as an effective interaction between two fermions mediated by the exchange of a spin-wave. The spin-wave propagators are $i\langle T e_q(t) e_q^\dagger(0) \rangle_\omega = (\Omega_q - \omega - i\delta)^{-1}$ and $i\langle T e_q^\dagger(t) e_q(0) \rangle_\omega = (\Omega_q + \omega - i\delta)^{-1}$, where $e_q^\dagger(e_q)$ are the boson creation (annihilation) operators, subindex ω implies Fourier transform, and the momentum \mathbf{q} runs over the whole Brillouin zone. A simple experimentation then shows that the forms of the two susceptibilities are reproduced if one chooses the following Hamiltonian for the interaction between the original fermionic operators and the magnons:

$$H_{el-mag} = \frac{2\Delta}{\sqrt{2S}} \sum'_k \sum_q \left[\eta_q c_{k+q, \alpha}^\dagger c_{k, \beta} (e_{-q}^\dagger + e_q) + \bar{\eta}_q c_{k+q, \alpha}^\dagger c_{k+Q, \beta} (e_{-q}^\dagger - e_q) \right] \delta_{\alpha, -\beta}. \quad (25)$$

Here and below a prime indicates that the summation is over the reduced Brillouin zone.

The expressions for η_q and $\bar{\eta}_q$ are

$$\eta_q = \frac{1}{\sqrt{2}} \left(\frac{1-\gamma_q}{1+\gamma_q} \right)^{1/4}, \quad \bar{\eta}_q = \frac{1}{\sqrt{2}} \left(\frac{1+\gamma_q}{1-\gamma_q} \right)^{1/4}. \quad (26)$$

Performing now the Bogolyubov transformation, we obtain the Hamiltonian for the interaction between the magnons and the conduction and valence band fermions

$$\begin{aligned}H_{el-mag} &= \sum'_k \sum_q (a_{i\alpha k}^\dagger a_{i\beta, k+q} e_q^\dagger \Phi_{aa}(k, q) + b_{i\alpha k}^\dagger b_{i\beta, k+q} e_q^\dagger \Phi_{bb}(k, q) \\ &+ a_{i\alpha k}^\dagger b_{i\beta, k+q} e_q^\dagger \Phi_{ab}(k, q) + b_{i\alpha k}^\dagger a_{i\beta, k+q} e_q^\dagger \Phi_{ba}(k, q) + \text{H.c.}) \delta_{\alpha, -\beta}.\end{aligned}\quad (27)$$

To leading order in t/U , the vertex functions are given by

$$\begin{aligned}\Phi_{aa,bb}(k, q) &= \left[\pm(\epsilon_k + \epsilon_{k+q})\eta_q + (\epsilon_k - \epsilon_{k+q})\bar{\eta}_q \right] \frac{1}{\sqrt{2S}}, \\ \Phi_{ab,ba}(k, q) &= 2\Delta \left[\eta_q \mp \bar{\eta}_q \right] \frac{1}{\sqrt{2S}}.\end{aligned}\tag{28}$$

We are now in a position to proceed systematically with the diagrammatic formulation of the two-magnon Raman scattering.

III. NONRESONANT SCATTERING

A. Raman matrix element

We start with the situation when the photon frequencies are much smaller than the gap, $\Delta \sim SU$. In this case, it has been shown²² that the Loudon-Fleury Hamiltonian¹⁴ gives a proper description of magnetic Raman scattering. We first show how this Hamiltonian can be reproduced in our momentum-space diagrammatic formalism. The key points in the derivation are the following: (i) to leading order in t/U the current operator necessarily transforms a valence fermion into the conduction one and *vice versa*; (ii) the vertex strength for a magnon emission accompanied by the fermion scattering from the valence to conduction band (and *vice versa*) is of order U , while for the fermion scattering *within* either the valence or conduction band, the vertex is of order t , i.e., much smaller (see Eq. (28)); (iii) for incoming/outgoing photon frequencies smaller than the gap, all the denominators in the diagrams are of the order of U . We can then identify three simple diagrams contributing towards the matrix element M_R of Eq. (10) to leading order in t/U . They are shown in Fig. 4. Notice that while the diagrams of Figs. 4(a),(b) have a superficial resemblance to those encountered in the theory of two-phonon Raman scattering in semiconductors,¹⁹ the diagram of Fig. 4(c) looks rather different. We will see shortly that the extra diagram is needed for the answer to have correct symmetry properties.

Performing the internal frequency integration in these three diagrams, we obtain

$$M_R^{(1)} = -4\mu_q\lambda_q \sum'_k \left(\frac{\partial\epsilon_k}{\partial\mathbf{k}} \cdot \hat{\mathbf{e}}_i \right) \left(\frac{\partial\epsilon_k}{\partial\mathbf{k}} \cdot \hat{\mathbf{e}}_f^* \right) \left(\frac{4\Delta}{4\Delta^2 - \Omega^2} + \frac{8\Delta(4\Delta^2 + \Omega^2)}{(4\Delta^2 - \Omega^2)^2} \right) \quad (29)$$

for the diagram in Fig. 4(b),

$$M_R^{(2)} = 4\mu_q\lambda_q \sum'_k \left(\frac{\partial\epsilon_k}{\partial\mathbf{k}} \cdot \hat{\mathbf{e}}_i \right) \left(\frac{\partial\epsilon_k}{\partial\mathbf{k}} \cdot \hat{\mathbf{e}}_f^* \right) \frac{8\Delta(4\Delta^2 + \Omega^2)}{(4\Delta^2 - \Omega^2)^2} \quad (30)$$

for the diagram in Fig. 4(c), and

$$M_R^{(3)} = 4(\mu_q^2 + \lambda_q^2) \sum'_k \left(\frac{\partial\epsilon_k}{\partial\mathbf{k}} \cdot \hat{\mathbf{e}}_i \right) \left(\frac{\partial\epsilon_{k-q}}{\partial\mathbf{k}} \cdot \hat{\mathbf{e}}_f^* \right) \left(\frac{4\Delta}{4\Delta^2 - \Omega^2} \right) \quad (31)$$

for the diagram in Fig. 4(a). In these three expressions Ω is a frequency equal to ω_i or ω_f . Specifying it more precisely at this stage is devoid of meaning since we would then have to take into account subleading diagrams in the t/U expansion. We also defined

$$\mu_q = \left[\frac{1}{2} \left(\frac{1}{\sqrt{1 - \gamma_q^2}} + 1 \right) \right]^{\frac{1}{2}}; \quad \lambda_q = \frac{\gamma_q}{|\gamma_q|} \left[\frac{1}{2} \left(\frac{1}{\sqrt{1 - \gamma_q^2}} - 1 \right) \right]^{\frac{1}{2}}. \quad (32)$$

These are related to η_q and $\bar{\eta}_q$ via

$$\sqrt{2}\mu_q = \bar{\eta}_q + \eta_q; \quad \sqrt{2}\lambda_q = (\bar{\eta}_q - \eta_q). \quad (33)$$

Adding up the above expressions, and taking into account that

$$\begin{aligned} & \sum'_k \left(\frac{\partial\epsilon_k}{\partial\mathbf{k}} \cdot \hat{\mathbf{e}}_i \right) \left(\frac{\partial\epsilon_{k-q}}{\partial\mathbf{k}} \cdot \hat{\mathbf{e}}_f^* \right) \\ &= \sum'_k (-2t)^2 [(\hat{\mathbf{x}} \sin k_x + \hat{\mathbf{y}} \sin k_y) \cdot \hat{\mathbf{e}}_i] [(\hat{\mathbf{x}} \sin(k_x - q_x) + \hat{\mathbf{y}} \sin(k_y - q_y)) \cdot \hat{\mathbf{e}}_f^*] \\ &= t^2 [e_{ix}e_{fx}^* \cos q_x + e_{iy}e_{fy}^* \cos q_y], \end{aligned} \quad (34)$$

we obtain for the Raman matrix element

$$M_R = -8t^2 \left[\frac{2\Delta}{4\Delta^2 - \omega^2} \right] [(e_{ix}e_{fx}^* + e_{iy}e_{fy}^*)2\mu_q\lambda_q - (e_{ix}e_{fx}^* \cos q_x + e_{iy}e_{fy}^* \cos q_y)(\mu_q^2 + \lambda_q^2)]. \quad (35)$$

We now demonstrate that this equation coincides with the Loudon-Fleury vertex. For this, we first rewrite the Loudon-Fleury Hamiltonian of Eq. (1) in terms of Holstein-Primakoff operators to leading order in $1/S$

$$\begin{aligned}
H_{LF} &= \alpha \sum_{r, \hat{\mu}=\{\hat{x}, \hat{y}\}} (\hat{\mathbf{e}}_i \cdot \hat{\boldsymbol{\mu}})(\hat{\mathbf{e}}_f^* \cdot \hat{\boldsymbol{\mu}}) \mathbf{S}_r \cdot \mathbf{S}_{r+\hat{\mu}} \\
&= \frac{\alpha}{2} \sum_r \left[e_{fx}^* e_{ix} \mathbf{S}_r \cdot (\mathbf{S}_{r+\hat{x}} + \mathbf{S}_{r-\hat{x}}) + e_{fy}^* e_{iy} \mathbf{S}_r \cdot (\mathbf{S}_{r+\hat{y}} + \mathbf{S}_{r-\hat{y}}) \right] \\
&= 2S\alpha \sum_q' \left\{ e_{fx}^* e_{ix} \left[\cos q_x (a_q a_{-q} + a_q^\dagger a_{-q}^\dagger) + 2a_q^\dagger a_q \right] \right. \\
&\quad \left. + e_{fy}^* e_{iy} \left[\cos q_y (a_q a_{-q} + a_q^\dagger a_{-q}^\dagger) + 2a_q^\dagger a_q \right] \right\}. \tag{36}
\end{aligned}$$

We then apply the Bogolyubov transformation to the actual magnon operators that diagonalize the Heisenberg model to first order in $1/S$. This transformation involves the same factors λ_q and μ_q that we had introduced earlier (in Eq. (32)) and has the form

$$\begin{aligned}
a_q^\dagger &= \mu_q e_q^\dagger - \lambda_q e_{-q}, \\
a_{-q} &= \mu_q e_{-q} - \lambda_q e_q^\dagger. \tag{37}
\end{aligned}$$

At $T = 0$ the only relevant terms in the Loudon-Fleury Hamiltonian are those containing two magnon creation operators, and restricting ourselves to those, we obtain the matrix element from the Loudon-Fleury Hamiltonian in the form

$$\begin{aligned}
M_R^{L-F} &= 2\alpha S \left\{ e_{fx}^* e_{ix} \left[\cos q_x (\lambda_q^2 + \mu_q^2) - 2\mu_q \lambda_q \right] \right. \\
&\quad \left. + e_{fy}^* e_{iy} \left[\cos q_y (\lambda_q^2 + \mu_q^2) - 2\mu_q \lambda_q \right] \right\}. \tag{38}
\end{aligned}$$

Comparing the two expressions for the Raman vertex, Eqs. (35) and (38), we observe that they coincide if one chooses $\alpha = 16t^2\Delta/[2S(4\Delta^2 - \omega^2)]$. Apart from the factor $2S$ ($= 1$ for $S = 1/2$), this is exactly the expression which Shastry and Shraiman obtained in their derivation of the Loudon-Fleury vertex for the Hubbard model.⁴⁵

Further, an examination of our diagrammatic derivation shows that the terms in Eq. (35) containing $\cos q_x$ and $\cos q_y$ correspond to the S^+S^- terms in the Loudon-Fleury Hamiltonian, while the rest of the terms come from the S^zS^z part. Going back to Eqs. (29), (30), and (31) and the diagrams they correspond to, we can see that the S^+S^- terms come from the diagram of Fig. 4(a), which emits one magnon from the hole line and other from the electron line. The S^zS^z terms come from the diagrams of Figs. 4(b),(c), which emit both magnons either from the electron or the hole side of the fermionic bubble. Notice that the ‘‘unusual’’

diagram of Fig. 4(c) canceled one of the terms in the one of Fig. 4(b). Without that cancellation we would not have obtained the correct Loudon-Fleury expression for the $S^z S^z$ term. This in particular would have resulted in a violation of the selection rule prohibiting the A_{1g} scattering.

There is an interesting parallel between this cancellation and one that occurs in the theory of two-phonon Raman scattering in semiconductors.¹⁹ In that case, there is a large cancellation between the two-phonon terms obtained by the iteration of a single-phonon—electron vertex, and the diagrams containing a single two-phonon—electron vertex. The cancellation in the phonon case is a consequence of the translational symmetry. In our case, the diagram of Fig. 4(c) can be seen as effectively containing a single two-magnon—fermion vertex. The partial cancellation due to this diagram restores the spin rotation invariance of the Loudon-Fleury Hamiltonian. It is then reasonable to assume that some cancellations may occur in higher orders in t/U , though we did not check this in explicit calculations.

Despite the agreement obtained between the two approaches, we are not done yet. We have so far been performing an expansion in t/U , and there exist other graphs which are of the same order in t/U as the ones retained. Examples are given in Fig. 5. However, it is not difficult to observe that all these extra diagrams have a smallness in $1/S$. Indeed, each fermion-magnon vertex has an overall factor of $1/\sqrt{2S}$ (see Eq. (28)). Associated with each internal magnon line, we have two such vertices, and *no* additional summation over the orbitals in the internal fermionic loop. Altogether, inclusion of an internal magnon line results in an extra factor of $1/2S$. This completes our demonstration of the equivalence of our formalism to that of Shastry and Shraiman in the non-resonant region.

B. Two-magnon peak

In the preceding subsection, we calculated the Raman matrix element M_R for the emission of two magnons. Here we consider the location and shape of the two-magnon peak. We first observe from Eq. (38) that within the Loudon-Fleury picture the scattering in the A_{1g}

geometry ($\hat{\mathbf{e}}_i = \frac{\hat{x}+\hat{y}}{\sqrt{2}}$, $\hat{\mathbf{e}}_f = \frac{\hat{x}-\hat{y}}{\sqrt{2}}$) vanishes because the Raman vertex M_R is equal to zero. This result can be expected because at half-filling (and at large U) the Hubbard model is equivalent to the Heisenberg model, and in the A_{1g} geometry the Loudon-Fleury and Heisenberg Hamiltonians commute with each other. On the contrary, in the B_{1g} scattering geometry ($\hat{\mathbf{e}}_i = \frac{\hat{x}+\hat{y}}{\sqrt{2}}$, $\hat{\mathbf{e}}_f = \frac{\hat{x}-\hat{y}}{\sqrt{2}}$) the Raman vertex, as obtained from Eq. (38), is finite

$$M_R^{B_1} \sim (\mu_q^2 + \lambda_q^2)(\cos q_x - \cos q_y) = \frac{\cos q_x - \cos q_y}{\sqrt{1 - \gamma_q^2}}. \quad (39)$$

Substituting this into the expression for Raman intensity, Eq. (9), we obtain

$$R^{B_1}(\omega) \sim \sum_q' \frac{(\cos q_x - \cos q_y)^2}{1 - \gamma_q^2} \delta(\omega - 2\Omega_q), \quad (40)$$

where $\omega = \omega_i - \omega_f$. This expression has a divergence near $\omega = 8JS$, since the magnon spectrum is flat and the density of states infinite at the Brillouine zone boundary. It is well-known, however, that this result changes qualitatively when one takes into account the effect of the magnon-magnon interactions in the final state. This was first explained by Elliott *et. al.*⁴⁶ and experimentally verified by Fleury⁴⁷ for RbMnF₃, which has a cubic structure. The calculations were further extended by Elliott and Thorpe.⁴⁸ They were performed for the two-dimensional case by Parkinson,⁴⁹ and then verified for K₂NiF₄ by Fleury and Guggenheim.⁵⁰ Since a rather up-to-date treatment of the role of the magnon-magnon interactions is available in the literature,^{6,16} we merely sketch the relevant calculations with an emphasis on the $1/S$ expansion, which treats the magnon-magnon interactions in a systematic way and which, to our knowledge, has not been discussed before in this context.

The standard way to treat the effects of multiple magnon-magnon scattering in the Raman problem is to write the Heisenberg Hamiltonian in terms of the Holstein-Primakoff bosons, diagonalize it, and keep only the interaction term $\sim \alpha_k^\dagger \beta_{-k}^\dagger \beta_{-l} \alpha_l$, which is responsible for multiple scattering of two magnons in the vacuum (Fig. 6). This is the procedure which Parkinson⁴⁹ and others used to derive the two-magnon Raman intensity. We note however that for arbitrary S , the restriction to only a single interaction term is not justified, as after the diagonalization of the quartic term in the Holstein-Primakoff bosons, one also obtains

processes of the form, say, $\alpha_k^\dagger \beta_{-k} \beta_{-l}^\dagger \alpha_l^\dagger$, which also contribute to the Raman intensity. The way to avoid this complication is, again, to study the large- S limit. The key point is that at infinite S the Raman intensity is divergent at $\omega = 2\Omega_q = 8JS$, which is the maximum possible two-magnon frequency. It is achieved when both magnons are right at the Brillouin zone boundary. At this boundary $\gamma_k = (\cos k_x + \cos k_y)/2 = 0$, and the anomalous term in the bosonic quadratic form in the Heisenberg antiferromagnet vanishes. In other words, the antiferromagnetic magnons right at the Brillouin zone boundary behave as free particles. Now, if S is large, the shift in the two-magnon Raman peak position due to the magnon-magnon interactions is small, so that one can still consider magnons as free particles and neglect the anomalous part in the quadratic form. In this situation, the only interaction term has two creation and two annihilation operators. Moreover, in the Raman problem the total momentum of two magnons is zero, and we can therefore write the interaction term in the truncated form

$$H_{int} = -\frac{8J}{N} \sum'_k \sum'_l \gamma_{k-l} \alpha_k^\dagger \beta_{-k}^\dagger \beta_{-l} \alpha_l. \quad (41)$$

The prime stands for summation over the magnetic Brillouin zone. We can further decompose

$$\gamma_{k-l} = \gamma_k \gamma_l + \tilde{\gamma}_k \tilde{\gamma}_l + \bar{\gamma}_k \bar{\gamma}_l + \tilde{\tilde{\gamma}}_k \tilde{\tilde{\gamma}}_l, \quad (42)$$

where the different symmetry factors are

$$\begin{aligned} \gamma_k &= \frac{1}{2}(\cos k_x + \cos k_y), & \tilde{\gamma}_k &= \frac{1}{2}(\cos k_x - \cos k_y), \\ \bar{\gamma}_k &= \frac{1}{2}(\sin k_x + \sin k_y), & \tilde{\tilde{\gamma}}_k &= \frac{1}{2}(\sin k_x - \sin k_y). \end{aligned} \quad (43)$$

For the B_{1g} scattering geometry, $M_R \propto \tilde{\gamma}_q$, and hence only $\tilde{\gamma}_k \tilde{\gamma}_l$ survives at each vertex. The remaining calculation of the series is straightforward, and we obtain for the Raman intensity

$$R_{B_{1g}}(\omega) \sim \text{Im} \left[\frac{I}{1 + \frac{1}{4S} I} \right], \quad (44)$$

where

$$I = \frac{1}{N} \sum'_q \frac{(\cos q_x - \cos q_y)^2}{\bar{\omega} - \bar{\Omega}_q + i\delta}, \quad (45)$$

and we introduced the reduced frequencies $\bar{\omega} = \omega/8JS$ and $\bar{\Omega}_q = \Omega_q/4JS$.

The imaginary part of Eq. (45) can be expressed in terms of complete elliptic integrals,

$$\text{Im } I = -\frac{8\bar{\omega}}{\pi\sqrt{1-\bar{\omega}^2}} \left[(2-\bar{\omega}^2)K(\bar{\omega}) - 2E(\bar{\omega}) \right]. \quad (46)$$

One can then express I via a dispersion relation,

$$I(\bar{\omega}) = \frac{8}{\pi^2} \int_0^1 d\nu \frac{\nu [(2-\nu^2)K(\nu) - 2E(\nu)]}{\sqrt{1-\nu^2} (\bar{\omega} - \nu + i\delta)}. \quad (47)$$

This one-dimensional integral is particularly convenient for a numerical evaluation of I .

For $S = \infty$ the denominator in Eq. (44) is irrelevant, and this expression reduces to (40), with the only difference in that we have set $\gamma_q \rightarrow 0$ in the M_R of Eq. (39), in order to be consistent with the approximations made in the derivation of the magnon-magnon interactions.

For large but finite S , the peak in the Raman intensity is located close to but not exactly at $\bar{\omega} = 1$. Expanding the integral in Eq. (45) in $1 - \bar{\omega}$, we obtain $I = A + iB$ where

$$A = -4 \frac{1 - \sqrt{1 - \bar{\omega}^2}}{\sqrt{1 - \bar{\omega}^2}}, \quad B = -\frac{4}{\pi} \frac{1}{\sqrt{1 - \bar{\omega}^2}} \log(1 - \bar{\omega}^2). \quad (48)$$

Substituting this into Eq. (44) we obtain after simple manipulations

$$R_{B_{1g}}(\bar{\omega}) \propto \frac{\sqrt{1 - \bar{\omega}^2} \log(1 - \bar{\omega}^2)}{\log^2(1 - \bar{\omega}^2) + \pi^2(1 - (S+1)(1 - \bar{\omega}))^2}. \quad (49)$$

We see that when the magnon-magnon interaction is included, $R_{B_{1g}}(\bar{\omega})$ no longer diverges but rather has a maximum at $\sqrt{1 - \bar{\omega}^2} \approx 2 \log(S+1)/(\pi(S+1))$. Moreover, right at the zone boundary Raman intensity turns to zero. If we formally set $S = 1/2$ in our $1/S$ expression for Raman intensity, Eq. (49), we obtain a peak centered at $\bar{\omega} = 0.696$ (or $\omega = 2.78J$). The peak position is close to the $\omega = 2.92J$ result obtained by Canali and Girvin.¹⁶ They used the same expression for I as we did and restricted to the same sequence of bubble diagrams, but they did not make a formal assumption of large S in their calculations of

intensity and therefore did not expand I in $1 - \bar{\omega}$ and set $\gamma_q = 1$ in (40). The agreement between our results and theirs shows that the two-magnon peak position is rather robust. On the other hand, the profile of the two-magnon peak depends strongly on at which stage in the calculations one extends a formal $1/S$ expansion to $S = 1/2$. We found that the use of the $1/S$ expansion results for A and B yield much broader peak than one obtains using the exact expression for I . This last form of the two-magnon profile is consistent with the results of numerical calculations¹⁵ and we therefore believe that it is closer to reality. The profile of the two-magnon intensity is plotted in Fig. 7.

Canali and Girvin also considered the effect of including the spin-wave velocity renormalization factor into the magnon propagator. To first order in $1/S$, this renormalization factor effectively shifts the value of J to $J_{eff} = J(1 + 0.16/2S)$. The same renormalization must indeed be present in our approach, so the position of the peak in our theory is at $\omega \sim 3.22J$.

The peculiar features of the two-magnon profile were first reported by Elliot and Thorpe⁴⁸ and Parkinson,⁴⁹ who performed the RPA summation without referring to the $1/S$ expansion, neglected spin-wave velocity renormalization and also kept the interaction terms with four creation and annihilation operators, which were assumed to have the same overall factor as in Eq. (41). For $S = 1/2$, a numerical solution of their equations yields a narrow peak at $\bar{\omega} = 0.675$ (i.e., $\omega = 2.7J$), which is not far from both our result and that of Canali and Girvin, though we believe that the restriction to a single interaction term is better justified as long as the virtual magnons are located near the Brillouin zone boundary.

Experimentally, the two-magnon peak has been observed in La_2CuO_4 at 3000 cm^{-1} (see Ref. 8), which for $\omega \sim 2.78J_{eff} \approx 3.22J$ yields $J \sim 0.116 \text{ eV}$ which is roughly consistent with $J \sim 0.125 \text{ eV}$ as inferred from the neutron scattering⁵¹ and NMR data.⁵² The Parkinson result corrected by the spin-wave velocity renormalization ($\omega = 2.7J_{eff} \approx 3.13J$) gives somewhat better agreement with the neutron data, but the difference between the two values of ω is rather small and practically irrelevant to subsequent analysis. In the rest of the paper, we will simply refer to $2.8J_{eff}$ for the two-magnon peak position.

We now proceed to the central topic of our paper, which is the discussion of Raman scattering in the resonant regime.

IV. RESONANT SCATTERING

A. Raman matrix element

In the section on non-resonant scattering we proceeded systematically in filtering out the diagrams that were small in t/U or $1/S$. Our very first step was to observe that the magnon-fermion vertex was of order U when the fermion scattered between the valence and conduction bands, and of order t when it scattered within either the valence or conduction band (see Eq. (28)). As the terms in the denominators obtained upon the internal frequency integration were always of order U , all the diagrams with intraband scattering at any magnon-fermion vertex were small by powers of t/U .

It turns out that this property of the denominators is no longer true in the resonant region, where the photon frequencies ω_i and ω_f differ from the gap 2Δ by quantities of order JS . As a result, some previously omitted diagrams become, as we will see, not only important, but actually dominant.

Let us first consider the form of the Raman spectrum without the final state interactions. Then we have

$$R(\omega) \propto \sum_q |M_R|^2 \delta(\omega_i - \omega_f - 2\Omega_q) \quad (50)$$

Consider now the graphs with only the intraband scattering at the fermion-magnon vertices, Fig. 8. With all the multiplicity factors included, the internal frequency integration results in

$$M_R^{(4)} = -8i \sum'_k \frac{\left(\frac{\partial \epsilon_k}{\partial \mathbf{k}} \cdot \hat{\mathbf{e}}_i\right) \left(\frac{\partial \epsilon_{k-q}}{\partial \mathbf{k}} \cdot \hat{\mathbf{e}}_f^*\right) [\mu_q \epsilon_{k-q} - \lambda_q \epsilon_k]^2}{(\omega_i - 2E_k + i\delta)(\omega_i - \Omega_q - E_k - E_{k-q} + i\delta)(\omega_f - 2E_{k-q} + i\delta)} \quad (51)$$

for the graph of Fig. 8(a), and

$$M_R^{(5)} = -8i \sum'_k \frac{\left(\frac{\partial \epsilon_k}{\partial \mathbf{k}} \cdot \hat{\mathbf{e}}_i\right) \left(\frac{\partial \epsilon_k}{\partial \mathbf{k}} \cdot \hat{\mathbf{e}}_f^*\right) [\mu_q \epsilon_{k-q} - \lambda_q \epsilon_k] [\mu_q \epsilon_k - \lambda_q \epsilon_{k-q}]}{(\omega_i - 2E_k + i\delta)(\omega_i - \Omega_q - E_k - E_{k-q} + i\delta)(\omega_f - 2E_k + i\delta)} \quad (52)$$

for the graph of Fig. 8(b). The relation $\omega_i - 2\Omega_q = \omega_f$ is to be remembered here.

Without performing the integrals, the naive order of magnitude estimate is obtained in the resonant region by assuming that the resonant terms in the denominators are of the order of the bandwidth, i.e., $\mathcal{O}(JS)$. Then the two diagrams above are of order $t^4/(JS)^3$. The diagrams that were dominant in the nonresonant region have fewer resonant denominators. Going back to Eq. (35) for the previously considered graphs, we find that they are of order $t^2/(2\Delta - \omega) \sim t^2/JS$. We see that in the resonant regime, the new diagrams are larger by a factor $(t/JS)^2 \sim U/J$. However, this estimate, while correct for the large- S case, can be somewhat misleading at the physically relevant value of $S = 1/2$, as it does not take into account strong self-energy and vertex corrections which are relevant at $\omega \approx 2\Delta$, even though we are considering the situation exactly at half-filling. For example, the leading order vertex correction to the magnon-fermion vertex, shown in Fig. 9(a), is of order $t(U/JS)^2$, whereas the bare vertex is of order t . Simultaneously, the self-energy correction in Fig. 9(b) contributes an extra factor of (U/JS) . Both corrections are small only if we require that $U/JS \ll 1$, which we indeed do not expect to be satisfied for $S = 1/2$.

The form of the low-energy theory at $U/JS \gg 1$, has been discussed by a number of authors. For our considerations, it is essential that both the numerical⁵³ and variational⁵⁴ studies have found that the resulting quasiparticle Green's function $G(\mathbf{k}, \omega)$ has a quasiparticle pole at low energies, and that the k -space dispersion of that quasiparticle has a width of order JS . Self-consistent calculations^{28,39,55} also demonstrated that the product of the quasiparticle residue Z and the effective (renormalized) interaction between quasiparticles U_{eff} scales as J (without corrections this product was equal to $U \times 1 = U$). In this situation, the relative factor between the new and the old diagrams is $U_{eff}Z/J = O(1)$. The order of magnitude estimates therefore only point to the new diagrams as being comparable in importance at resonance to those that fully dominated away from the resonance.

Fortunately, this naive order of magnitude estimate is not the whole story. When the

integrals are actually performed, they may (and as we will see, they do) yield singular answers for some photon and/or magnon frequencies. In that case, the most singular integral will dominate. Notice that because the singularity comes only from the coherent part of the quasiparticle spectral weight $A(\mathbf{k}, \omega)$, we do not need to consider incoherent part of $A(\mathbf{k}, \omega)$, which by itself can be substantial and spread over the energy scale exceeding J (some studies predict that $A(\mathbf{k}, \omega)$ spreads over the scale of the order $J \left(\frac{t}{J}\right)^\gamma$, where γ is a number ≤ 1).

We now consider in detail the singular behavior of various diagrams. The diagrams which contribute to the Loudon-Fleury Hamiltonian have only singly resonant denominators that lead to singularity in M_R when either the incoming or the outgoing photon frequency coincides either with the gap, 2Δ , or with the top of the band.⁵⁶ Near the gap, the integration over the intermediate momenta yields $M_R \sim |\omega_{i,f} - 2\Delta|^{-1/2}$ for the mean-field form of the quasiparticle dispersion, or an even weaker logarithmic singularity $M_R \sim \log 1/|\omega_{i,f} - 2\Delta|$ for the renormalized quasiparticle spectrum, which has minima at $(\pm\pi/2, \pm\pi/2)$ and a parabolic dispersion around the minima. This last form of the fermionic spectrum was obtained in the numerical, variational, and perturbative studies of the Hubbard model beyond the mean-field level.^{28,39,44} Near the top of the band ($\mathbf{k} \approx \mathbf{0}$), there would be logarithmic singularity due to the vanishing of the denominator is in fact absent because $\frac{\partial \epsilon_{\mathbf{k}}}{\partial \mathbf{k}}$ in the numerator of M_R also vanishes at $\mathbf{k} = \mathbf{0}$.

Consider next the diagram in Fig. 8(a). Its analytical expression is given by Eq. (51). The denominator in Eq. (51) has three terms, one of which is half of the sum of the other two⁵⁷

$$\omega_i - \Omega_q - E_k - E_{k+q} = \frac{1}{2} [(\omega_i - 2E_k) + (\omega_f - 2E_{k+q})]. \quad (53)$$

Therefore, if we find \mathbf{k} and \mathbf{q} such that $\omega_i = 2E_k$ and $\omega_f = 2E_{k+q}$, all three of the denominators in (51) vanish simultaneously. This is known as triple resonance, which is a particular case of the more general notion of multiple resonance known in Raman scattering.^{19,20} Clearly, a necessary condition for a triple resonance is that the fermionic bandwidth be larger than the magnon bandwidth. This condition is satisfied in the mean-field theory, where the

magnon bandwidth is $4JS$, while the fermionic bandwidth, found from

$$E_k \simeq \Delta + 2JS(\cos k_x + \cos k_y)^2, \quad (54)$$

is equal to $8JS$. The bandwidths of “dressed” Fermi and Bose quasiparticles are indeed somewhat different, but we assume that the fermionic bandwidth is still larger than the magnon bandwidth.

We will present a detailed study of the momentum integration near the triple resonance in the next subsection, and here merely note that, unlike its single counterpart, the triple resonance is not tied to the minimum of either E_k or E_{k+q} . Thus, unlike for the Loudon-Fleury terms, for triple resonance the difference between the mean-field and the renormalized forms of the quasiparticle spectrum does not yield qualitatively different answers for the singularities. For this reason, we will keep working with the mean-field form of E_k . In the next subsection we will find that triple resonance does indeed yield the strongest divergence of the Raman scattering cross-section.

Finally, in the diagram of Fig. 8(b), we have a product of $(\omega_i - 2E_k)$, $(\omega_f - 2E_k)$, and their half-sum in the denominator. Since $\omega_f = \omega_i - 2\Omega_q$, only one of the three terms can vanish at any time, and this diagram is clearly less singular than the one with the triple resonance.

In fact, there are also higher order diagrams which have internal magnon lines or contain four-fermion vertices in low orders. They may formally be even more singular than the ones above. However, just as in the nonresonant section, we can omit them if we assume the large- S limit, which was implicit in the considerations just outlined.

B. Triple resonance

In this subsection, we perform a detailed analysis of the diagram of Fig. 8(a), which gives rise to a triple resonance. The analytical expression for the diagram was given in Eq. (51).

It may be useful to start with a remark on the related calculations of the two-phonon spectra in semiconductors. In that case the energy scale of the phonons is quite small compared

to the bandwidth in semiconductors. Therefore an expansion of electronic band structure to quadratic order near the minima is *a priori* warranted, and the resulting integrals are often doable analytically.^{19,58,59}

In our case, however, the wavevectors of the magnons contributing to the two-magnon peak are of the same order as the Brillouin zone itself, and their energy is comparable to the fermionic bandwidth. Thus, we are forced to deal with a full spin density wave band structure without necessarily being able to expand it near some point. This complicates the integration considerably, although we will eventually find that some analytical results are still possible.

We now turn to the general analysis of the possible singularities in Eq. (51).

As we mentioned earlier, the three denominators in Eq. (51) vanish simultaneously when the following two conditions hold,

$$\omega_i = 2E_k; \quad \omega_f = \omega_i - 2\Omega_q = 2E_{k+q}. \quad (55)$$

Let us call \mathbf{k}_0 the value of \mathbf{k} that solves the above equations, and expand the denominators to linear order about \mathbf{k}_0 . To study the conditions for a resonance, we set the numerator to a constant and obtain

$$M_R^{(4)} \sim \int d^2k \frac{1}{(2\mathbf{v}_{k_0} \cdot \mathbf{k} - i\delta)((\mathbf{v}_{k_0} + \mathbf{v}_{k_0-q}) \cdot \mathbf{k} - i\delta)(2\mathbf{v}_{k_0-q} \cdot \mathbf{k} - i\delta)} \quad (56)$$

where $\mathbf{v}_{k_0} = \frac{\partial E_k}{\partial \mathbf{k}}|_{k_0}$ and $\mathbf{v}_{k_0-q} = \frac{\partial E_k}{\partial \mathbf{k}}|_{k_0-q}$ are the velocities at the two points in the momentum space where the denominators vanish.

We now immediately see that this integral vanishes unless the two velocities are strictly antiparallel to each other. Indeed, let \mathbf{v}_{k_0} be in the x -direction. Then the first term in the denominator only depends on k_x . If \mathbf{v}_{k_0-q} has a y -component, then only the second and third terms in the denominator will contain k_y , and both *with the same sign*. In that case, if we do the k_y integration first, the integral will vanish since the poles from both terms will lie in the same half-plane.

The condition for the velocities at \mathbf{k}_0 and $(\mathbf{k}_0 - \mathbf{q})$ to be antiparallel has a simple physical interpretation⁵⁹ in the semiclassical picture, where both momenta and coordinates can be

assigned to the quasiparticle wavepackets. Suppose the incoming photon creates a particle-hole pair at $\mathbf{k} = \pm\mathbf{k}_0$. The energies of particles and holes have different signs, so that the resulting electron and hole run apart with velocities $+\mathbf{v}_{k_0}$ and $-\mathbf{v}_{k_0}$, respectively. After the emission of two magnons, with the momenta $\pm\mathbf{q}$, the electron and hole velocities become $\pm\mathbf{v}_{k_0-q}$. Only if the electron and hole are “aimed back” at the point of origin, will they recombine to emit a final photon. Thus \mathbf{v}_{k_0-q} has to be antiparallel to \mathbf{v}_{k_0} .

Let us now count the variables in our equations for the resonance. For fixed ω_i and ω_f we have two resonance conditions, an additional condition that the two velocities be antiparallel, and also the energy conservation condition $2\Omega_q = \omega \equiv \omega_i - \omega_f$. Thus, we have four equations for four unknown components of \mathbf{k}_0 and \mathbf{q} . However, at a fixed ω_i this system of four equations does not necessarily have a solution for an arbitrary ω_f . For example, for the rotationally invariant magnon spectrum and parabolic fermionic bands, elementary considerations show that the two conditions in Eq. (55) plus the energy conservation condition fully determine $|\mathbf{k}_0|$, $|\mathbf{q}|$, and the angle between them, so for a fixed ω_i the condition on velocities has a solution only at a *single* ω_f , and for that one ω_f *all* of the magnons are at resonance at once. In the general case, the magnon spectrum is not rotationally invariant, but the triple resonance will still occur only in some range of the final photon energies ω_f (and thus only for some magnon energies Ω_q). We will find that this range is numerically rather narrow in most cases of interest.

We now study the general solution for triple resonance. Consider first the mean-field ($S = \infty$) forms of the fermion and magnon dispersions. We expand $2E_k = 2\sqrt{\Delta^2 + 4t^2(\cos k_x + \cos k_y)^2} \simeq 2\Delta + 4JS(\cos k_x + \cos k_y)^2$ and introduce the reduced variables

$$\lambda_i = \frac{\omega_i - 2\Delta}{4JS}, \quad \lambda_f = \frac{\omega_f - 2\Delta}{4JS}, \quad (57)$$

which count the photon energies from the band edge. Then Eq. (55) becomes

$$\cos k_x + \cos k_y = \sqrt{\lambda_i}, \quad \cos l_x + \cos l_y = \sqrt{\lambda_f}, \quad (58)$$

where $\mathbf{k} \equiv \mathbf{k}_0$, and where we introduced $\mathbf{l} = \mathbf{k} - \mathbf{q}$ and also restricted ourselves to the reduced Brillouin zone.

The condition that the velocities $\frac{\partial E_k}{\partial \mathbf{k}}$ and $\frac{\partial E_l}{\partial \mathbf{l}}$ be antiparallel is

$$\sin k_x \sin l_y - \sin l_x \sin k_y = 0, \quad (59)$$

provided that if \mathbf{k} is in the first quadrant, then \mathbf{l} is in the third (this makes the velocities *antiparallel*).

Finally, the condition $E_k - E_l = 2\Omega_{k-l}$ takes the form

$$2\sqrt{1 - \frac{1}{4}(\cos(k_x - l_x) + \cos(k_y - l_y))^2} = \lambda_i - \lambda_f. \quad (60)$$

These four coupled nonlinear equations is the set to deal with. There exists no general method for solving systems of nonlinear equations. However, in our particular case, much information can be obtained analytically by studying two high symmetry directions, which we do next.

Let us first consider the case where $q_x = q_y$. It is easy to check that for such \mathbf{q} , the solution for the resonance has a general form $k_x = k_y$ ($0 < k_x < \pi/2$) and $l_x = l_y$ ($-\pi/2 < l_x < 0$). The antiparallel velocities condition is automatically satisfied, and the remaining conditions yield

$$\begin{aligned} \cos k_x &= \frac{\sqrt{\lambda_i}}{2}, & \cos l_x &= \frac{\sqrt{\lambda_f}}{2}, \\ 2\sqrt{1 - \cos^2(k_x - l_x)} &= 2\sin(k_x - l_x) = \lambda_i - \lambda_f. \end{aligned} \quad (61)$$

These three equations trivially lead to

$$\bar{\Omega}_q = \frac{1}{4} \left[\lambda_i - 2 + \sqrt{3\lambda_i(4 - \lambda_i)} \right], \quad (62)$$

where as before $\bar{\Omega}_q = \frac{\Omega_q}{4JS}$ is a reduced magnon frequency.

By definition, the upper limit on λ_i is equal to 4. The lower limit is found by locating the point where $\lambda_f = \lambda_i - 2\bar{\Omega}_q$ becomes zero, since at that point one of the velocities vanishes, and after that we have parallel rather than antiparallel velocities and thus no contribution

from the triple resonance to the Raman vertex. Solving $\lambda_i = 2\bar{\Omega}_q$ together with Eq. (62) we find the lower boundary is at $\bar{\Omega}_q = 1/2$, $\lambda_i = 1$. Eq. (62) is graphically presented in Fig. 10.

Another symmetry direction for which the condition on the velocities is satisfied automatically is that for which \mathbf{q} is along the x or y -axis. In this case we can set $k_y = l_y = q_y = 0$, and obtain a set of equations

$$\begin{aligned}\lambda_i &= (1 + \cos k_x)^2, & \lambda_f &= (1 + \cos l_x)^2, \\ \lambda_i - \lambda_f &= 2\sqrt{1 - \frac{1}{4}(1 + \cos(k_x - l_x))^2}.\end{aligned}\tag{63}$$

It actually does lead to an analytic answer, but as it is rather cumbersome, we refrain from presenting it and consider instead only two special points. The first one is where the magnon energy is maximal, i.e., $\lambda_i - \lambda_f = 2$. This implies $k_x - l_x = \pi$, and hence $\lambda_i = 9/4$. The second special point is one at which $\lambda_f = 0$, i.e., the termination point on the lower end. At that point $l_x = -\pi$, and we easily obtain from Eq. (63) that

$$\lambda_i(\lambda_i + 1)^2 = 16,\tag{64}$$

with the solution $\lambda_i \simeq 1.9$.

The whole curve⁶⁰ $\omega_q = f(\lambda_i)$ for $q_x = 0$ is plotted in Fig. 10.

Another part that is worth deriving analytically is the locus of the lower and upper termination points of the curves for different directions of \mathbf{q} . It is easy to demonstrate that for the largest possible $\lambda_i = 4$, the solution for any direction is $\lambda_f = 3$, so that the curves for all directions of \mathbf{q} meet at a single point when $\lambda_i = 4$. To see this, note that $\lambda_i = 4$ implies $k_x = k_y = 0$. After substituting this into Eqs. (58), (59), and (60), we obtain the claimed result.

The lower termination point is $\lambda_f = 0$, because the triple resonance clearly requires both the initial and final photon frequencies to lie above the gap. This condition corresponds to a straight line given by $\lambda_i = 2\bar{\omega} = (\omega_i - \omega_f)/4JS$ in the $(\lambda_i, \bar{\omega})$ plane (recall that at resonance, $\bar{\omega} = \bar{\Omega}_q$). This by itself would allow $0 < \lambda_i < 2$. A more detailed study shows, however, that the solution only exists for $\lambda_i > 1$. Notice that curves for different magnon

directions terminate at different points on the line $\lambda_i = 2\bar{\omega}$, and near $\lambda_i = 1$ only a small fraction of magnon directions, namely $q_x \approx q_y$, allow a triple resonance there (see Fig. 10). At the other end of this boundary (at $\lambda_i = 2$), the numerator in (51) vanishes. For all these reasons, Raman intensity is expected to be small in the region of low λ_i , and it will not play any role in our subsequent analysis.

Finally, we can also locate the region where our set of equations has a solution for the largest possible magnon frequency $\bar{\omega} = \bar{\Omega}_q = 1$. An inspection of Eqs. (58), (59), and (60) shows that the solution exists for $2 < \lambda_i < 3$.

Combining all these analytical results, we obtain the allowed region of triple resonances in the $(\lambda_i, 2\bar{\omega})$ plane. This region is shaded in Fig. 10. Notice that although for $2 < \lambda_i < 3$ the solid line in the figure (the solution for $q_x = 0$) practically coincides with the horizontal line $2\bar{\omega} = 2\bar{\Omega}_q = 2$, this solid line is actually located *below* the maximum two-magnon frequency everywhere except $\lambda_i = 9/4$. As an independent check, we also solved our equations numerically for a number of directions of \mathbf{q} and found that the solutions were within the shaded region.

The above solution for the triple resonance was obtained for the mean-field forms of fermionic and magnon dispersions. As we already discussed, quantum corrections will certainly change the overall scales in the dispersions and thus modify the resonance conditions. However, we do not expect these modifications to be substantial especially near the upper termination point $\lambda_i = 4$ as still, at maximum λ_i we have $k_x = k_y = 0$, and hence curves with different directions of q will terminate at the same λ_i . This region near maximum λ_i will play central role in our subsequent analysis.

Finally, it is worth noticing that the divergence we have found in Raman matrix element is an artifact of neglecting the damping of quasiparticles. If the damping was included, the divergence would be gone, and we would obtain instead only the enhancement of M_R in the shaded region in Fig. 10. For this reason, later in the paper we will refer to an enhancement rather than to a singularity in M_R . It is important, however, that up to some damping levels the enhancement of M_R is going to be substantial, and the singularity analysis is a useful

guide to the actual physics.

C. Two-magnon scattering

So far we have considered the behavior of the Raman matrix element as a function of incoming frequency, neglecting finite state interaction, and selected the diagram which gives rise to a strong enhancement of M_R in some range of outgoing photon frequencies for a given ω_i . At the same time, as we discussed in Sec. III B, the density of states is divergent at the magnetic zone boundary, and in the absence of finite state interaction this naturally gives rise to a divergence of R at $\omega = 8JS$. For $S = 1/2$, which we will assume below, this divergence is at $\omega = 4J$.

If we now switch on the magnon-magnon interactions, the divergence at $4J$ will be gone, and we will obtain instead the maximum of R at a smaller frequency. In principle, this frequency should be different from that obtained in Sec. III B, as the Raman matrix element in Eq. (51) has a complicated dependence on the magnon momentum \mathbf{q} , and the terms in the resulting series problem cannot be factorized. On the other hand, the location of the two-magnon peak at about $3J$ is in agreement with the experimental^{8,13} as well as numerical data.^{6,15,61} If so, the influence of the \mathbf{q} -dependence of M_R on the magnon-magnon scattering should not be substantial. There will be also a feedback effect from the magnon-magnon scattering on the location of the region where the Raman matrix element is enhanced due to triple resonance. However, this feedback effect will be small in the semiclassical (large S) approximation, which, as we discussed in Sec. III B, is likely to work well even for $S = 1/2$. For all these reasons, for the rest of our discussion we adopt a semiphenomenological approach and assume that at any given ω_i the Raman spectrum $R(\omega)$ has two *independent* peaks: one is due to the triple resonance, which is particularly relevant to the first diagram in Fig. 6 which has no finite state interaction, and the other, which for definiteness we assume to be at $\omega = 2.8J_{eff}$, is due to the magnon-magnon scattering (all other diagrams in Fig. 6). In essence, the approximation we made implies that

we are considering an “effective” Loudon-Fleury-like model, in which the Raman vertex is considered as constant in the calculations of the two-magnon peak position, but the overall magnitude of the vertex does indeed strongly depend on how close we are to the triple resonance region.

Without considering in detail the effects of damping, we cannot conclude which of the two peaks is stronger. The experiments seem to indicate that the peak at $2.8J_{eff}$ is stronger, and the enhancement of the Raman matrix element can only be responsible for the asymmetric “shoulder-like” behavior of the two-magnon profile (see the discussion in Sec. V). At the same time, if we fix ω at $2.8J_{eff}$, as in Fig. 2, and consider the variation of the two-magnon peak intensity as a function of the incident photon frequency ω_i (or λ_i), this intensity will clearly have a maximum where an $\omega = const$ line intersects the region of the triple resonance.

To see where the maximum occurs, we neglect for simplicity the renormalization of J due to quantum fluctuations and draw a horizontal line in Fig. 10 at the reduced frequency $\bar{\omega} = 0.7$ (we checked that the results below are practically insensitive to whether we use J or J_{eff} in the magnon spectrum; however, if we used J_{eff} , we would also have to consider the $1/S$ renormalization for the fermionic spectrum, which does not lead to new physics but substantially complicates the calculations). We see from the figure that the line at $\bar{\omega} = 0.7$ intersects the region of triple resonances in two places. One occurs at λ_i very close to 4, i.e., when the incident photon is near the *top* of the fermionic band. The other occurs for λ_i close to 1, i.e., not far from the *bottom* of the fermionic band. We know from the discussion given above that the region $1 < \lambda_i < 2$, especially for λ_i close to 1, is rather “esoteric” in that only a small fraction of magnon directions allow for a triple resonance there (see Fig. 10). On the other hand, for λ_i close to 4, we will encounter no such problem, and we thus expect a much larger enhancement there. Thus, we focus entirely on the latter value of $\lambda_i \approx 4$.

We now consider how the two-magnon peak amplitude increases as ω_i approaches the critical value where the triple resonance and the magnon-magnon peak occur at the same value of $\bar{\omega}$. First, since we are close to the top of the fermionic band, we can perform a quadratic expansion of the band structure near the maximum. Second, we see from Fig. 10

that near $\lambda_i = 4$, the triple resonance region is very narrow, so that to first approximation we can consider that the triple resonance occurs only along a single line in the $(\lambda_i, \bar{\omega})$ plane. As we discussed in Sec. IV B, this would have been the case if the magnon spectrum was rotationally invariant, and one can easily check that it approximately is for $\bar{\Omega}_q \sim 0.7$. Accordingly, we expect it to be a good approximation if we linearize the magnon spectrum around $\mathbf{q} = \mathbf{0}$,

$$\bar{\Omega}_q \simeq \frac{q}{\sqrt{2}}. \quad (65)$$

The integral for the triple resonance can now be done analytically. The details of the calculations are presented in the Appendix. Here we quote the results. The resonance is allowed at the line

$$\lambda_i = 4 - (\bar{\omega} - \frac{1}{2})^2, \quad (66)$$

which, in accordance with Fig. 10, terminates at $\lambda_i = 4$ for $\bar{\omega} = 1/2$, and intersects the two-magnon peak position ($\bar{\omega} = 0.7$) at $\lambda_i = \lambda_i^{res} = 3.96$. The maximum of the two-magnon peak amplitude thus corresponds to the incoming photon frequency ω_i that puts the particle-hole pair members very close to the tops of their respective bands.

Let us now fix the two-magnon frequency at the two-magnon peak position and vary λ_i (as in Fig. 2). From the results in the Appendix, the Raman matrix element is then

$$M_R \sim \frac{4 - \lambda_i}{(\lambda_i - \lambda_i^{res} + i\delta)^{3/2}} \quad (67)$$

The factor in the numerator comes from the vanishing of the term $\frac{\partial \epsilon_{\mathbf{k}}}{\partial \mathbf{k}}$ in the numerator of Eq. (51) at $\mathbf{k} = \mathbf{0}$, which is the value of \mathbf{k} of the resonant particle-hole pair created by the incoming photon for $\lambda_i = 4$, and also due to the fact that $\lambda_i = 4$ corresponds to $\bar{\Omega}_q - \frac{1}{2} = 0$ in which case the overall factor $(1 - \frac{\bar{\Omega}_q}{q^2}) \equiv (1 - \frac{1}{2\bar{\Omega}_q})$ in Eq. (92) in the Appendix vanishes.

For λ_i very close to λ_i^{res} , the term in the numerator can be considered as a constant, and we obtain

$$M_R \sim \frac{1}{[\lambda_i - \lambda_i^{res} + i\delta]^{3/2}}. \quad (68)$$

In practice, however, the damping of fermions prevents the true singularity at $\lambda_i = \lambda_i^{res}$, and the increase of M_R can be measured at some distance away from λ_i^{res} . In this situation, the difference between λ_i^{res} and 4 can be neglected, and we obtain from (67)

$$M_R \sim \frac{1}{(\lambda_i - \lambda_i^{res} + i\delta)^{1/2}}, \quad (69)$$

The sum total of those arguments is that the Raman intensity has *at least* an inverse linear singularity from triple resonance.

$$R \sim [\lambda_i - \lambda_i^{res} + i\delta]^{-1}. \quad (70)$$

It is important to note that the usual single (Loudon-Fleury) resonance in 2D can *at best* give an inverse linear singularity of R for the spin density wave band structure, and only at the mean field level, due to the degeneracy of $E_k = \sqrt{\Delta^2 + \epsilon_k^2}$. Once the mean-field degeneracy is broken by a better approximation, the single resonance is further reduced to a logarithmic singularity. Therefore the triple resonance singularity is expected to be at least as strong, and most likely stronger than any at the lower band edge.

This is to be contrasted with the behavior of the optical conductivity $\sigma(\omega)$ (see Eq. (22) above and Fig. 11(a)). Unlike the Raman cross-section, it vanishes at the upper band edge $\lambda_i = 4$. Most of the optical weight in $\sigma(\lambda_i)$ is concentrated towards the lower band edge $\lambda_i = 0$, where it has a singularity in the absence of fermionic damping. Therefore, the optical conductivity resonates at the lower band edge while the Raman cross-section is strongest at the upper band edge of the coherent quasiparticle spectrum.

Notice also that while the Raman intensity is symmetric with respect to the sign of $\lambda_i - \lambda_i^{res}$, the expression (67) for M_R , which includes only the leading singularity, is, strictly speaking, valid only in some region around λ_i^{res} . Away from this region, there are no reasons to expect the Raman intensity to be symmetric. On general grounds, we expect that the intensity above λ_i^{res} must fall down faster than for the same deviation from λ_i^{res} but at $\lambda_i < \lambda_i^{res}$ simply because no triple resonance is possible for $\lambda_i > 4$.

We now discuss in more detail how these (and other) results are related to experiment.

V. DISCUSSION

We first summarize the main results of our work.

We developed a general diagrammatic approach to Raman scattering in antiferromagnetic insulators. For photon frequencies small compared to the gap between conduction and valence band, we rederived diagrammatically the Loudon-Fleury Hamiltonian,¹⁴ which had been first derived from the Hubbard model by Shastry and Shraiman²² in a different formalism. We also considered the location and shape of the two-magnon peak by studying the magnon-magnon scattering in a systematic $1/S$ expansion. The results of this study are consistent with the earlier considerations by Canali and Girvin.¹⁶

We studied for the first time the two-magnon Raman scattering in the so-called resonant regime when the incident and final photon frequencies are only $\mathcal{O}(J)$ apart from the Hubbard gap. In this situation, the diagrams which are subleading in the nonresonant region become dominant. We identified the diagram which gave a dominant contribution to the Raman vertex in the resonant regime, and found the region in the $(\omega_i, \omega_i - \omega_f)$ plane where the Raman vertex is divergent, unless one includes into consideration the damping of quasiparticles. The divergence is due to the simultaneous vanishing of all three denominators in the expression for the Raman matrix element. This phenomenon is called triple resonance. In the presence of a moderate quasiparticle damping, the divergence in the Raman vertex is gone, but the enhancement due to the triple resonance can indeed survive.

Based on the experimental data, we then assumed that the location of the two-magnon peak in the resonant regime remains practically in the same place as at small photon frequencies, i.e., at $\omega_i - \omega_f \sim 3J$. For nearly all incoming photon frequencies ω_i falling within the Hubbard bands (i.e., corresponding to the features in the optical absorption spectrum), this magnon frequency is located below the region where our calculations show a triple resonance is allowed (see Fig. (10)). Based on these facts, we formulated an “effective” Loudon-Fleury-like theory in which the position and shape of the Raman profile in the two-magnon peak area of ≈ 3000 *cm* (but not at higher magnon frequencies) is solely due to the

final state magnon-magnon interactions, while the triple resonance in the Raman vertex at larger $\omega \sim 4000 \text{ cm}^{-1}$ leads to the “shoulder-like” behavior in the magnon profile. When the incident photon frequency approaches $\omega_i^{max} = 2\Delta + 8J$, which corresponds to the particle and the hole being excited to nearly the tops of their respective bands, the triple resonance region allowed at a given ω_i shifts down to lower transferred frequencies, and finally intersects the value of ω where the two-magnon peak is located. We found that this happens when $\omega_i/2$ is very close to the top of the quasiparticle band, $\omega_i = \omega_i^{res} \approx \omega_i^{max}$. Right at the crossing point, the intensity of the two-magnon peak amplitude diverges (in the absence of quasiparticle damping).

As ω_i approaches this critical value from below, the Raman intensity increases as $R \sim (\omega_i^{res} - \omega_i)^{-1}$ at some distance away from the resonance, and as $R \sim (\omega_i^{res} - \omega_i)^{-3}$ in the immediate vicinity of the resonance. In a real situation, the true divergence will be gone due to damping of quasiparticles, and the two-magnon peak intensity as a function of ω_i will instead have a maximum at ω_i^{res} . We therefore do not expect to see cubic dependence, but inverse linear increase of R should be observable.

We now analyze how these results are related to the experimental measurements in Fig. 1 and Fig. 2. In the Introduction we listed the key experimental features that required explanation. Here we list them again and comment on each of them.

In Fig. 1:

(a) *Asymmetry of the two-magnon peak profile*: our theory predicts that for ω smaller than ω_i^{res} the two-magnon peak profile should be asymmetric with a “shoulder-like” behavior at frequencies close to $\omega = 4J$, due to the triple resonance in the Raman vertex. This is consistent with experimental observations. In particular, the experimentally measured two-magnon profile in Pr_2CuO_4 was analyzed¹² and found to contain two peaks, a two-magnon peak at 3000 cm^{-1} , and a smaller one at 4000 cm^{-1} , which is precisely as expected from our calculations. Notice, however, that the calculation of the relative intensity of the peaks is beyond the scope of the present approach.

(b) *Selection rules*: The leading diagram in the resonance regime contributes to scattering

in both B_{1g} and A_{1g} geometries. The signals in both geometries have been observed in the experiments. Recall that the Loudon-Fleury theory predicts scattering only in the B_{1g} geometry.

(c) *Stability of the two-magnon peak profile:* Away from the resonance, the stability of the two-magnon peak profile is consistent with our theory, as the enhancement of the Raman vertex for $2 < \lambda_i < 3.5$ occurs near $\omega = 4J$. As ω_i approaches ω_i^{res} , the situation becomes more complex, as one cannot separately consider the peak due to magnon-magnon interaction and the enhancement of the Raman vertex due to the triple resonance. The experimental data seem to indicate that the two-magnon peak profile changes little as ω_i sweeps through the resonance. This is not entirely consistent with our scenario, as the triple resonance region shifts to lower magnon energies ω as the photon frequency ω_i approaches ω_i^{res} . However, the magnon profile itself in the resonant region can only be obtained by solving coupled equations for the enhancements due to the triple resonance and the final state magnon-magnon interactions. We have not yet been able to accomplish that, and we leave it for future work. We regard this as the most important unresolved issue of all that remain. Notice also that the observed distortion of the Raman profile at higher photon frequencies is qualitatively consistent with our main conclusion that once the photon frequency passes the top of the coherent quasiparticle band, one must consider a qualitatively different set of electronic states. Our speculation at present is that at such frequencies the dominant contribution to Raman scattering comes from an incoherent, diffusive hole motion, which can more easily couple to multi-magnon excitations.

In Fig. 2:

(a) *A single peak:* Our theory predicts a *single* maximum in the two-magnon peak intensity measured as a function of the incident photon frequency. On the contrary, on the basis of general considerations in Raman scattering,¹⁹ we might have expected two peaks, one at $\omega_i = 2\Delta$, and the other at $\omega_f = 2\Delta$. These are the so-called incoming and outgoing resonances. In the more traditional area of phonon Raman scattering in semiconductors,^{19,20,63} the two peaks are not always separately resolved. However, given the large magnon energy scale in

the cuprates, we might have expected them to be resolvable. An additional bit of evidence that triple resonance is a plausible explanation is that, experimentally, the two-magnon peak is seen in the interval of incoming photon frequencies about 4000 cm^{-1} in width, which for $J \sim 1000 \text{ cm}^{-1}$ is of the same width as the interval $2 < \lambda_i < 4$ in our theory, where the triple resonance is possible for all directions of the magnon momenta \mathbf{q} .

(b) *Peak location:* Our theory predicts the maximum of the two-magnon peak intensity, measured as a function of ω_i , right near the upper edge of the quasiparticle fermionic band. At the same time, the coherent quasiparticle contribution to the optical conductivity $\sigma(\omega)$ was shown to have most of its weight located near the lower band edge and vanish at the upper band edge (as schematically illustrated in Fig. 11(b)). This is consistent with the experimental Fig. 2 which shows that Raman scattering is strongest right at the upper end of those features in the optical data that can be interpreted as particle-hole excitations between the lower and upper Hubbard bands. The location of the Raman maximum versus the features in $\sigma(\omega)$ has been one of the greatest experimental puzzles in this area, and its solution in our approach serves as a partial verification of the SDW dispersion relation for the carriers which, despite much theoretical work, has not been well-established experimentally in these materials.

In Fig. 12 we fit the published experimental data¹⁸ from Fig. 2 on the peak intensity in $YB_2Cu_3O_6$ at room temperature by our Eq. (70). We see that a fit to the predicted inverse linear dependence is reasonably good. The inverse linear dependence starts from $\omega_i \sim 2.4 \text{ eV}$ and extends nearly up to the resonance frequency $\omega_i^{res} \approx 3.1 \text{ eV}$. The effects of fermionic damping are probably relevant only in the immediate vicinity of the resonance. Note that the resonance value obtained from the fit is larger than the peak location at $\omega_i^{res} \sim 2.8 \text{ eV}$ in Fig 2. In fact, the experimental data at high frequencies have been reexamined in recent studies⁶⁵. It turns out that the resonance at room temperature occurs at a higher frequency than has been previously believed, and in particular the the intensity at $\omega_i \sim 2.9 \text{ eV}$ is found to be *larger* than at $\omega_i \sim 2.8 \text{ eV}$, unlike what one sees in Fig. 2. The new data suggest the resonance frequency value may exceed 3 eV , which would make it even more consistent with

the fit to the theoretical dependence.

These recent experiments⁶⁵ also measured the peak intensity in $YB_2Cu_3O_{6.1}$ at low temperatures ($T \sim 5K$). We fitted the new data by the same inverse linear dependence and found even better agreement with the experimental data for ω_i between 2.5 eV and 3 eV. This fit yields about the same resonance frequency $\omega_i^{res} \sim 3.1$ eV as the fit at room temperatures. We actually do not expect that the resonance values at room temperatures and at 5K are the same, but we notice that the optical studies in La_2CuO_4 have shown⁶⁴ that the optical absorption peak shifts to higher frequencies by less than 0.1 eV between room temperatures and 122 K, and one can expect the peak in Raman intensity to shift by about the same amount. This small shift is indeed within the combined accuracy of our theory and the data available for the fits.

Notice that our theory also predicts that the Raman intensity should have an additional, smaller, peak at $\omega \sim 2\Delta \sim 1.7$ eV due to the Loudon-Fleury mechanism. There is no evidence for the peak at $\omega_i = 2\Delta$ in the room temperature data on Fig 2. Preliminary results of recent low-temperature experiments⁶⁶ indicate a possibility that there is in fact a second, smaller peak at $\omega_i \sim 1.6$ eV which is consistent with our prediction.

There are, however, several experimental results which are beyond the scope of our approach. First is the width of the two-magnon peak, which exceeds the prediction of the spin-wave theory even if we take into account the resonance in the Raman vertex. As we already remarked above, simply invoking quantum fluctuations for spin-1/2 is unlikely to improve the spin-wave theory, since direct numerical calculations of the Raman spectrum on finite clusters also predict a narrow peak in this case.⁶¹ Another experimental fact is the existence of a considerable Raman signal $R(\omega)$ above the maximum possible two-magnon energy (i.e., above $4J_{eff}$). Canali and Girvin¹⁶ performed a very detailed study of the effects of four-magnon scattering within the context of the Heisenberg model for spins and the Loudon-Fleury coupling of spins to light. They found that this scattering can give rise to the Raman cross-section above $4J_{eff}$, but the intensity of the Raman signal was found to be too small to fully account for the experimental data. Thus one apparently has to go

beyond the minimal model.

In the approach put forward by Singh,^{6,15} further neighbor terms in the effective Hamiltonian for coupling of light to spins are postulated, and the coefficients adjusted so that the moments of the Raman spectrum evaluated by the series expansion agree with observations. Such next-nearest-neighbor terms broaden the two-magnon peak and also automatically break the selection rule for the Loudon-Fleury Hamiltonian which disallows scattering in the A_{1g} configuration. Of course, a question then arises of the origin of such terms and their relative strength. Notice that the further-neighbor terms are in fact also effectively present in our momentum-space description, as it clearly follows from the Shraiman-Shastry formulation of the problem in which the non-Loudon-Fleury terms in the Raman vertex correspond to the effective spin interactions between further neighbors.

In the bulk of the paper we “factorized” the problem by setting the Raman vertex to its Loudon-Fleury form in the calculations of two-magnon profile right near the peak. This, however, is only an approximation, and in view of Singh’s results, we can expect some broadening of the two-magnon peak in the more sophisticated calculations along our lines, which would treat the resonance and the final state interactions together. Simultaneously, we might also expect a shift of the two-magnon peak position from $2.8J_{eff}$. In the bulk of the paper we used $2.8J_{eff}$ because of the agreement with neutron experiments. We note however, that the only observations to date of the two-magnon peak in cuprates were made at or near the resonant frequencies, which are in the visible light region in cuprates. In that sense, we may not even know what the “true”, i.e., nonresonant peak shape and location are.

The scattering in B_{1g} and A_{1g} geometries in the SDW technique has been studied by Kampf and Brenig.²³ They, however, focused on high *transferred* frequencies, comparable to the Mott-Hubbard gap, and did not include collective spin fluctuation modes (i.e., magnons) in their theory. In view of this, a comparison of our results with theirs is not possible.

In a rather different spirit, it was observed in a paper by Weber and Ford⁶⁷ that even a rather small magnon damping introduced phenomenologically into the equations broaden’s

the Parkinson peak considerably. More recently, Merlin⁶⁸ argued that phonons may be the source of that damping. Should the electron-phonon interaction prove relevant to the problem, this will only lend credence of the key phenomenological assumption of this work, namely that on a “first pass” at the resonant scattering problem, it is best not to try to deal simultaneously with two quite possibly distinct issues of the two-magnon peak shape and its strength variation with the incoming photon frequency.

Finally, an experimental fact which needs answering is the existence of the Raman signal at *very* high incident and transferred frequencies, of the order of 3.5 eV and 1 eV, respectively. The largest intensity at such high frequencies was obtained in the “chiral” A_{2g} channel. Khveshchenko and Wiegmann recently performed an elegant study of the contribution to Raman vertex in this frequency range from chiral spin fluctuations in the magnetically ordered phase.⁶⁹ For our considerations, it is essential that at such high frequencies, the incoming photon is above the coherent quasiparticle band (where our theory applies) and the motion of the carriers that subsequently couple to the magnons is itself incoherent in character. This and other interesting issues require further experimental data as well as an improved theoretical understanding.

VI. ACKNOWLEDGEMENTS

It is our pleasure to thank G. Blumberg, C. Canali, S. L. Cooper, D. Khveshchenko, M. V. Klein, R. Liu, R. Martin, R. Merlin, H. Monien, D. Pines, S. Sachdev, C. M. Varma, P. Wiegmann, and A. Zawadowski for useful discussions and comments. We are grateful to G. Blumberg, M. V. Klein, S. L. Cooper and R. Liu for providing experimental data for our Figs. 1, 2, and 12. D.F. is supported by the Texas Center for Superconductivity at the University of Houston. Part of the work has been done while A.C. was at Yale University, where he was supported by the National Science Foundation (NSF) Grant Nos. DMR-8857228 and DMR-9224290, and while D. F. was at the University of Illinois, where he was supported by the NSF (DMR 91-20000) through the Science and Technology Center

for Superconductivity at the University of Illinois at Urbana-Champaign.

VII. APPENDIX

In this Appendix, we obtain Eq. (67) for the Raman matrix element near the intersection between $\omega = 2.8J_{eff}$, where the two-magnon peak occurs, and a (narrow) region in the $(\lambda_i, \bar{\omega})$ plane where triple resonance is allowed. For simplicity, we will neglect the difference between J and J_{eff} . We see from Fig. 10 that this intersection occurs very close to the top of the quasiparticle fermionic band $E_k = (\Delta^2 + 4t^2(\cos k_x + \cos k_y)^2)^{1/2}$, i.e., near $\mathbf{k} = \mathbf{0}$. Once this is established for this band structure, we can get a good approximation for the integrals by expanding the energies to quadratic order around $\mathbf{k} = \mathbf{0}$.

The integral of interest is Eq. (51) for the diagram in Fig. 8(a):

$$M_R = -8i \sum'_k \frac{\left(\frac{\partial \epsilon_k}{\partial \mathbf{k}} \cdot \hat{\mathbf{e}}_i\right) \left(\frac{\partial \epsilon_{k-q}}{\partial \mathbf{k}} \cdot \hat{\mathbf{e}}_f^*\right) [\mu_q \epsilon_{k-q} - \lambda_q \epsilon_k]^2}{(\omega_i - 2E_k + i\delta)(\omega_f - 2E_{k-q} + i\delta)(\omega_i - \Omega_q - E_k - E_{k-q} + i\delta)} \quad (71)$$

We have upon expanding

$$\epsilon_k = -2t(\cos k_x + \cos k_y) \simeq -4t \left(1 - \frac{\mathbf{k}^2}{4}\right), \quad (72)$$

and (we consider $S = 1/2$)

$$E_k = \sqrt{\Delta^2 + \epsilon_k^2} \simeq \Delta + 4J \left(1 - \frac{\mathbf{k}^2}{2}\right). \quad (73)$$

We will expand both E_k and E_{k+q} , which implies that we also assume that the typical magnon momenta are not too large. This, as we discuss in the bulk of the paper, is consistent with our explicit result that the width of the region where triple resonance is allowed is very narrow, nearly a single line. To the same accuracy we can also linearize the magnon spectrum, $\Omega_q = \sqrt{2}Jq$. However, we found it convenient to keep using the general form Ω_q for the magnon frequency in some of the formulae.

To study the singular behavior, we first set the numerator to a constant. Expanding in powers of \mathbf{k} in (73) and introducing, as before, the reduced variables, $\lambda_i = (\omega_i - 2\Delta)/2J$, $\lambda_f = (\omega_f - 2\Delta)/2J$, and $\bar{\Omega}_q = \Omega_q/2J$, we obtain the following integral,

$$I = \int d^2k \frac{1}{(\lambda_i - 4 + 2\mathbf{k}^2 + i\delta)(\lambda_f - 4 + 2(\mathbf{k} - \mathbf{q})^2 + i\delta)(\lambda_i - \bar{\Omega}_q - 4 + \mathbf{k}^2 + (\mathbf{k} - \mathbf{q})^2 + i\delta)}. \quad (74)$$

Somewhat similar integrals appear in the three-dimensional problem of two-phonon resonant Raman scattering, where the incoming photon frequency is tuned to match the critical points in the semiconductor band structure. The case when the hole band has an infinite mass was done analytically by R. Martin.⁵⁹ The case of equal effective masses in two dimensions has not, to our knowledge, been studied analytically before, and we present the derivation in some detail.

We first observe that one of the terms in the denominator of the integrand is half the sum of two others. The integrand can thus be put in the form

$$\frac{1}{AB \left(\frac{A+B}{2}\right)} = \frac{1}{2 \left(\frac{A+B}{2}\right)^2} \left(\frac{1}{A} + \frac{1}{B}\right). \quad (75)$$

We now recall Feynman identity familiar from Quantum Electrodynamics,

$$\frac{1}{P^2Q} = \int_0^1 dx \frac{2x}{(xP + (1-x)Q)^3}. \quad (76)$$

Using this identity and completing the squares containing \mathbf{k} , as necessary, we obtain

$$I = \int d^2k \int_0^1 dx \left[\frac{x}{\left(\lambda_i - 4 + i\delta - x\bar{\Omega}_q - \left(\frac{x^2}{2} - x\right)q^2 + 2\left(\mathbf{k} - \frac{x}{2}\mathbf{q}\right)^2\right)^3} + \frac{x}{\left(\lambda_i - 4 + i\delta - (2-x)\bar{\Omega}_q - \left(\frac{x^2}{2} - x\right)q^2 + 2\left(\mathbf{k} - \left(1 - \frac{x}{2}\right)\mathbf{q}\right)^2\right)^3} \right]. \quad (77)$$

Shifting the variables of integration and using the integral

$$\int d^2k \frac{1}{(S + 2k^2)^3} = \frac{\pi}{4S^2}, \quad (78)$$

we obtain

$$I = \frac{\pi}{4} \int_0^1 dx \left[\frac{x}{\left(\lambda_i - 4 + i\delta - x\bar{\Omega}_q - \left(\frac{x^2}{2} - x\right)q^2\right)^2} + \frac{x}{\left(\lambda_i - 4 + i\delta - (2-x)\bar{\Omega}_q - \left(\frac{x^2}{2} - x\right)q^2\right)^2} \right]. \quad (79)$$

Completing further the squares with respect to the variable of integration x , we rewrite the r.h.s. of (79) as $I = I_1 + I_2$, where

$$\begin{aligned} I_1 &= \frac{\pi}{4} \int_0^1 dx \frac{x}{\left[\lambda_i - 4 + \frac{q^2}{2} \left(1 - \frac{\bar{\Omega}_q}{q^2} \right)^2 + i\delta - \frac{q^2}{2} \left(x - \left(1 - \frac{\bar{\Omega}_q}{q^2} \right) \right) \right]^2}, \\ I_2 &= \frac{\pi}{4} \int_0^1 dx \frac{x}{\left[\lambda_i - 4 + \frac{q^2}{2} \left(1 - \frac{\bar{\Omega}_q}{q^2} \right)^2 + i\delta - \frac{q^2}{2} \left(x - \left(1 + \frac{\bar{\Omega}_q}{q^2} \right) \right) \right]^2}. \end{aligned} \quad (80)$$

At this stage, we have reduced I to two integrals of the general type

$$J = \int_0^1 dx \frac{x}{[C - F^2(x - D)]^2}. \quad (81)$$

In both I_1 and I_2 , we have the same

$$C = \lambda_i - 4 + \frac{q^2}{2} \left(1 - \frac{\bar{\Omega}_q}{q^2} \right)^2 + i\delta \quad (82)$$

and $F^2 = \frac{q^2}{2}$. However, the D 's are not the same. We have

$$D_1 = \left(1 - \frac{\bar{\Omega}_q}{q^2} \right), \quad (83)$$

and

$$D_2 = \left(1 + \frac{\bar{\Omega}_q}{q^2} \right) \quad (84)$$

in I_1 and I_2 , respectively.

We now rewrite J as

$$J = \int_0^1 dx \frac{x - D}{[C - F^2(x - D)]^2} - \frac{\partial}{\partial C} \int_0^1 dx \frac{D}{C - F^2(x - D)^2}. \quad (85)$$

Performing the integrations and partial differentiation with respect to parameter, we obtain

$$J = \frac{1}{2F^2} \frac{1}{(C - F^2(x - D)^2)} \Big|_0^1 + \frac{D}{2C} \frac{x - D}{(C - F^2(x - D)^2)} \Big|_0^1 + \frac{D}{4F} \frac{1}{C^{\frac{3}{2}}} \log \left(\frac{F(x - D) + \sqrt{C}}{F(x - D) - \sqrt{C}} \right) \Big|_0^1. \quad (86)$$

The integral I is a sum of two such integrals and is thus

$$\begin{aligned}
I = I_1 + I_2 = \frac{\pi}{4} \left\{ \frac{1}{2F^2} \frac{1}{(C - F^2(x - D_1)^2)} \Big|_0^1 + \frac{1}{2F^2} \frac{1}{(C - F^2(x - D_2)^2)} \Big|_0^1 \right. \\
+ \frac{D_1}{2C} \frac{x - D_1}{(C - F^2(x - D_1)^2)} \Big|_0^1 + \frac{D_2}{2C} \frac{x - D_2}{(C - F^2(x - D_2)^2)} \Big|_0^1 \\
\left. + \frac{D_1}{4F} \frac{1}{C^{\frac{3}{2}}} \log \left(\frac{F(x - D_1) + \sqrt{C}}{F(x - D_1) - \sqrt{C}} \right) \Big|_0^1 + \frac{D_2}{4F} \frac{1}{C^{\frac{3}{2}}} \log \left(\frac{F(x - D_2) + \sqrt{C}}{F(x - D_2) - \sqrt{C}} \right) \Big|_0^1 \right\}. \quad (87)
\end{aligned}$$

It turns out that the first four terms inside the braces add up to zero. To see this, we observe that the definitions of D_1 and D_2 given above imply that

$$(1 - D_1) = -(1 - D_2), \quad (88)$$

which in turn implies that $(1 - D_1)^2 = (1 - D_2)^2$, and

$$\frac{D_1}{2(1 - D_1)} + \frac{D_2}{2(1 - D_2)} + 1 = 0. \quad (89)$$

We also use the identity

$$\frac{1}{C} \frac{1}{(C - P)} = \left(\frac{1}{C - P} - \frac{1}{C} \right) \frac{1}{P} \quad (90)$$

whenever terms of this type occur. Using all these identities, we can easily show by a direct calculation the cancellation claimed above.

We now have a compact result

$$I = \frac{\pi}{4} \frac{1}{C^{\frac{3}{2}}} \left\{ \frac{D_1}{4F} \log \left(\frac{F(x - D_1) + \sqrt{C}}{F(x - D_1) - \sqrt{C}} \right) \Big|_0^1 + \frac{D_2}{4F} \log \left(\frac{F(x - D_2) + \sqrt{C}}{F(x - D_2) - \sqrt{C}} \right) \Big|_0^1 \right\}. \quad (91)$$

Substituting the full expressions for D_1 , D_2 , and F , we obtain

$$\begin{aligned}
I = \frac{\pi}{4} \frac{1}{C^{\frac{3}{2}}} \left\{ \frac{(1 - \frac{\bar{\Omega}_q}{q^2})}{2\sqrt{2}q} \left[\log \left(\frac{1 + \frac{\sqrt{2}q}{\Omega_q} \sqrt{C}}{1 - \frac{\sqrt{2}q}{\Omega_q} \sqrt{C}} \right) - \log \left(\frac{1 - \frac{\sqrt{2}}{q(1 - \frac{\bar{\Omega}_q}{q^2})} \sqrt{C}}{1 + \frac{\sqrt{2}}{q(1 - \frac{\bar{\Omega}_q}{q^2})} \sqrt{C}} \right) - 2\pi i \right] \right. \\
\left. + \frac{(1 + \frac{\bar{\Omega}_q}{q^2})}{2\sqrt{2}q} \left[\log \left(\frac{1 - \frac{\sqrt{2}q}{\Omega_q} \sqrt{C}}{1 + \frac{\sqrt{2}q}{\Omega_q} \sqrt{C}} \right) - \log \left(\frac{1 - \frac{\sqrt{2}}{q(1 + \frac{\bar{\Omega}_q}{q^2})} \sqrt{C}}{1 + \frac{\sqrt{2}}{q(1 + \frac{\bar{\Omega}_q}{q^2})} \sqrt{C}} \right) \right] \right\}. \quad (92)
\end{aligned}$$

The vanishing of C corresponds to the triple resonance. Near this point, I behaves as $I \sim C^{-\frac{3}{2}}$.

The expression above is incomplete until we specify the branches of the logarithms and the square roots. A careful examination of the derivation shows that we must choose the square root branch which is positive for $C > 0$ and the branch of the logarithms which tends to zero when its argument goes to unity. The answer for other real values of C is obtained by setting $C \rightarrow C + i\delta$ and then analytically continuing C along the real axis.

We now turn to the form-factor in the numerator of Eq. (71). Clearly, for any $\lambda_i^{res} < 4$, this form-factor can be considered constant in the immediate vicinity of λ_i^{res} . At the same time, since the form-factor vanishes at the top of the quasiparticle band, it will contribute a small factor to Raman intensity for $\lambda_i^{res} \sim 4$. This will effectively change the singularity of the Raman matrix element at some distance away from the triple resonance, since for λ_i away from 4 the difference between λ_i^{res} being exactly 4 or merely close to it is not noticeable.

Near $\lambda_i^{res} = 4$, we set $(\mu_q \epsilon_{k-q} - \lambda_q \epsilon_k) = const$, linearize $\frac{\partial \epsilon_k}{\partial \mathbf{k}} \sim \mathbf{k}$ and $\frac{\partial \epsilon_{k-q}}{\partial \mathbf{k}} \sim \mathbf{k} - \mathbf{q}$, expand the numerator terms to quadratic order, and obtain

$$M_R \sim \sum_k' \frac{[\mathbf{k} \cdot \hat{\mathbf{e}}_i][(\mathbf{k} - \mathbf{q}) \cdot \hat{\mathbf{e}}_f^*]}{(\lambda_i - 4 + 2\mathbf{k}^2 + i\delta)(\lambda_f - 4 + 2(\mathbf{k} - \mathbf{q})^2 + i\delta)(\lambda_i - \bar{\Omega}_q - 4 + \mathbf{k}^2 + (\mathbf{k} - \mathbf{q})^2 + i\delta)} \quad (93)$$

in place of Eq. (74) above. Then we proceed using Feynman parametric representation as in the case with a constant numerator above. The two shifted \mathbf{k} variables in Eq. (77) were $\mathbf{k}' = \mathbf{k} - \frac{x}{2}\mathbf{q}$ and $\mathbf{k}'' = \mathbf{k} - \left(1 - \frac{x}{2}\right)\mathbf{q}$. We can alternately express the numerator in the integral above in terms of these as

$$[\mathbf{k} \cdot \hat{\mathbf{e}}_i][(\mathbf{k} - \mathbf{q}) \cdot \hat{\mathbf{e}}_f^*] = \left[\left(\mathbf{k}' + \frac{x}{2}\mathbf{q} \right) \cdot \hat{\mathbf{e}}_i \right] \left[\left(\mathbf{k}' - \left(1 - \frac{x}{2} \right) \mathbf{q} \right) \cdot \hat{\mathbf{e}}_f^* \right], \quad (94)$$

and

$$[\mathbf{k} \cdot \hat{\mathbf{e}}_i][(\mathbf{k} - \mathbf{q}) \cdot \hat{\mathbf{e}}_f^*] = \left[\left(\mathbf{k}'' + \left(1 - \frac{x}{2} \right) \mathbf{q} \right) \cdot \hat{\mathbf{e}}_i \right] \left[\left(\mathbf{k}'' - \frac{x}{2}\mathbf{q} \right) \cdot \hat{\mathbf{e}}_f^* \right]. \quad (95)$$

When we now integrate over \mathbf{k}' and \mathbf{k}'' in the B_{1g} scattering geometry, the angular integrals will only leave the terms $-\frac{x}{2}(1 - \frac{x}{2})(\mathbf{q} \cdot \hat{\mathbf{e}}_i)(\mathbf{q} \cdot \hat{\mathbf{e}}_f^*)$ in the numerator. Thus, we obtain the same integrals as in Eq. (80) above, except that instead of x in the numerators

we will have $-\frac{x^2}{2}(1-\frac{x}{2})$. The angular factor involving magnon momenta, $(\mathbf{q}\cdot\hat{\mathbf{e}}_i)(\mathbf{q}\cdot\hat{\mathbf{e}}_f^*)$, when computed in the B_{1g} geometry, is just an expansion of the Loudon-Fleury vertex $M_R^{B_1}$ of Eq. (39) to quadratic order in \mathbf{q} , which is consistent with the linearization of the form-factor done in the beginning of this calculation.

The integrals over the parametric variable x can now be done by elementary means similar to those employed above for a constant numerator case. The resulting expressions are, however, too lengthy to be worth presenting here. At the same time, as we discussed above, what is of real interest to us is the modification of the singular behavior of M_R at the values of λ_i at which one can neglect the difference between $\lambda_i - \lambda_i^{res}$ and $\lambda_i - 4$. A simplest way to proceed is to consider the case $\lambda_i^{res} = 4$, when we also have $\bar{\Omega}_q = \frac{1}{2}$. In that case $D_1 = 0$ in Eq. (83), and $D_2 = 2$ in Eq. (84). Thus, of the two integrals like the one of Eq. (81) above, but now with $-\frac{x^2}{2}(1-\frac{x}{2})$ instead of x in the numerator, only the one with D_1 is singular for small C . The singularity is, furthermore, picked up near $x = 0$, so that we can also omit the factor $(1-\frac{x}{2})$ in the numerator. We end up with

$$M_R \sim \int_0^1 \frac{x^2}{[4C - x^2]^2}, \quad (96)$$

with $C = \lambda_i - 4 + i\delta$.

Performing an elementary integration, and omitting an irrelevant nonsingular term, we obtain

$$M_R \sim \frac{2}{\sqrt{C}} \left(\ln \left(\frac{1 - 2\sqrt{C}}{1 + 2\sqrt{C}} \right) + i\pi \right), \quad (97)$$

which has a leading square root singularity $\frac{2\pi i}{\sqrt{C}}$. This is the result needed in the main text. Combining now Eqs. (92) and (97) and restricting to only a leading singularity, we obtain the result quoted in Eq. (67) in the main text.

REFERENCES

* Present address.

- ¹ P. W. Anderson, *Science* **235**, 1196 (1987).
- ² P. W. Anderson and J. R. Schrieffer, *Physics Today* **44**(6), 54 (1991), and references therein.
- ³ See the discussion by P. W. Anderson, D. Pines, and D. J. Scalapino in *Physics Today* **47**(2), 9 (1994); also a column in *Science* **261**, 294 (1993).
- ⁴ R. Merlin, *Journal de Physique (Paris), Colloque C5*, **41**, C5-233 (1980).
- ⁵ M. G. Cottam and D. L. Lockwood, *Light Scattering in Magnetic Solids* (Wiley, New York, 1986).
- ⁶ R. R. P. Singh, *Comments Cond. Mat. Phys.* **15**, 241 (1991).
- ⁷ S. L. Cooper, M. V. Klein, *Comments Cond. Mat. Phys.* **15**, 99 (1990).
- ⁸ K. B. Lyons, P. A. Fleury, L. T. Schneemeyer, and J. V. Waszczak, *Phys. Rev. Lett.* **60**, 732 (1988).
- ⁹ K. B. Lyons, P. A. Fleury, J. P. Remeika, A. S. Cooper, and T. J. Negran, *Phys. Rev. B* **37**, 2353 (1988).
- ¹⁰ S. Sugai, S. Shamoto, and M. Sato, *Phys. Rev. B* **38**, 6436 (1988).
- ¹¹ P. E. Sulewsky, P. A. Fleury, K. B. Lyons, S.-W. Cheong, and Z. Fisk, *Phys. Rev. B* **41**, 225 (1990).
- ¹² I. Tomeno, M. Yoshida, K. Ikeda, K. Tai, K. Takamuku, N. Koshizuka, S. Tanaka, K. Oka, and H. Unoki, *Phys. Rev. B* **43**, 3009 (1991).
- ¹³ G. Blumberg, R. Liu, M. V. Klein, W. C. Lee, D. M. Ginsberg, C. Gu, B. W. Veal, and B. Dabrowski, *Phys. Rev. B* **49**, 13296 (1994).

- ¹⁴ P. A. Fleury and R. Loudon, Phys. Rev. **166**, 514 (1968).
- ¹⁵ R. R. P. Singh, P. A. Fleury, K. B. Lyons, and P. E. Sulewski, Phys. Rev. Lett. **62**, 2736 (1989).
- ¹⁶ C. M. Canali and S. M. Girvin, Phys. Rev. B **45**, 7127 (1992).
- ¹⁷ M. Yoshida, S. Tajima, N. Koshizuka, S. Tanaka, S. Uchida, and T. Itoh, Phys. Rev. B **46**, 6505 (1992).
- ¹⁸ R. Liu, M. V. Klein, D. Salamon, S. L. Cooper, W. C. Lee, S. W. Cheong, D. M. Ginsberg, J. Phys. Chem. Solids **54**, 1347 (1993).
- ¹⁹ M. Cardona, in *Light Scattering in Solids II*, M. Cardona and G. Güntherodt, eds. (Springer-Verlag, New York, 1982).
- ²⁰ R. M. Martin and L. M. Falikov, in *Light Scattering in Solids*, M. Cardona, ed. (Springer-Verlag, New York, 1975).
- ²¹ E. T. Heyen, J. Kircher, and M. Cardona, Phys. Rev. B **45**, 3037 (1992).
- ²² B. S. Shastry and B. I. Shraiman, Phys. Rev. Lett. **65**, 1068 (1990); Int. J. Mod. Phys. B **5**, 365 (1991).
- ²³ A. P. Kampf and W. Brenig, Ann. Physik **1**, 206 (1992); Z. Phys. B **89**, 313 (1992).
- ²⁴ N. Bulut, D.J. Scalapino and S.R. White, Phys. Rev. Lett **73**, 748 (1994).
- ²⁵ J. R. Schrieffer, X. G. Wen, and S. C. Zhang, Phys. Rev. B **39**, 11663 (1989).
- ²⁶ S. Sachdev, Phys. Rev. B **39**, 12232 (1989).
- ²⁷ S. Trugman, Phys. Rev. B **37**, 1597 (1988); Phys. Rev. B **41**, 892 (1990).
- ²⁸ C. L. Kane, P. A. Lee, and N. Read, Phys. Rev. B **39**, 6880 (1989).
- ²⁹ B. I. Shraiman and E. D. Siggia, Phys. Rev. B **42**, 2485 (1990); V. Elser, D. Huse, B. I.

- Shraiman, and E. D. Siggia, Phys. Rev. B **41**, 6715 (1990).
- ³⁰ S. Schmitt-Rink, C. M. Varma, and A. E. Ruckenstein, Phys. Rev. Lett. **60**, 2793 (1988).
- ³¹ J. Zhong and H.-B. Shüttler, Phys. Rev. Lett. **69**, 1600 (1992).
- ³² K. Yonemitsu, A. R. Bishop, and J. Lorenzana, Phys. Rev. Lett. **69**, 965 (1992).
- ³³ C. M. Varma, private communication.
- ³⁴ F. C. Zhang and T. M. Rice, Phys. Rev. B **37**, 3759 (1988).
- ³⁵ S. B. Bacci, R. Gagliano, R. M. Martin, and J. F. Annett, Phys. Rev. B **44**, 7504 (1991).
- ³⁶ M. S. Hybertsen, E. B. Stechel, M. Schluter, and D. R. Jennison, Phys. Rev. B **41**, 11068 (1990).
- ³⁷ S. L. Cooper, private communication.
- ³⁸ Q. Si, Y. Zha, K. Levin, and J.P. Lu, Phys. Rev. B **47**, 9055 (1993), and references therein.
- ³⁹ A. V. Chubukov and D. M. Frenkel, Phys. Rev. B **46**, 11884 (1992).
- ⁴⁰ A. V. Chubukov and K. Musaelian, Phys. Rev. B, to appear.
- ⁴¹ A. V. Chubukov and D. M. Frenkel, Phys. Rev. Lett., to appear.
- ⁴² For full details, including the geometric factors, see W. Hayes and R. Loudon, *Scattering of Light by Crystals* (Wiley-Interscience, New York, 1978), and references therein.
- ⁴³ I. Affleck and F. D. M. Haldane, Phys. Rev. B **36**, 5291 (1987).
- ⁴⁴ A. Singh and Z. Tesanovic, Phys. Rev. B **41**, 11457 (1990); G. Vignale and M. R. Hedayati, Phys. Rev. B **42**, 786 (1990); A. Singh, Phys. Rev. B **43**, 3617 (1991); H. Monien and K. S. Bedell, Phys. Rev. B **45**, 3164 (1992); A. V. Chubukov and K. Musaelian, Phys. Rev. B **50**, 6238 (1994).
- ⁴⁵ We corrected a trivial factor of 4 in Ref. 22.

- ⁴⁶ R. J. Elliott, M. F. Thorpe, G. F. Imbush, R. Loudon, and J. B. Parkinson, *Phys. Rev. Lett.* **21**, 147 (1968).
- ⁴⁷ P. A. Fleury, *Phys. Rev. Lett.* **21**, 151 (1968).
- ⁴⁸ R. J. Elliott and M. F. Thorpe, *J. Phys. C* **2**, 1630 (1969).
- ⁴⁹ J. B. Parkinson, *J. Phys. C* **2**, 2012 (1969).
- ⁵⁰ P. A. Fleury and H. J. Guggenheim, *Phys. Rev. Lett.* **24**, 1346 (1970).
- ⁵¹ S. M. Hayden, G. Aeppli, H. Mook, D. Rytz, M. F. Hundley, and Z. Fisk, *Phys. Rev. Lett.* **67**, 3622 (1991).
- ⁵² T. Imai, C. P. Slichter, K. Yoshimura, and K. Kosuge, *Phys. Rev. Lett* **70**, 1002 (1993).
- ⁵³ V. Elser, D. Huse, B. I. Shraiman, and E. D. Siggia, *Phys. Rev. B* **41**, 6715 (1990); E. Dagotto, R. Joynt, A. Moreo, S. Bacci, and E. Gagliano, *Phys. Rev. B* **41**, 9049 (1990).
- ⁵⁴ S. Trugman, *Phys. Rev. B* **37**, 1597 (1988); **41**, 892 (1990); S. Sachdev, *Phys. Rev. B* **39**, 12232 (1989).
- ⁵⁵ O. P. Sushkov, *Phys. Rev. B* **49**, 1250 (1994).
- ⁵⁶ Actually, each of the diagrams (a) and (b) in Fig. 4 also has a term with a doubly resonant denominator. However, the doubly resonant terms cancel when we add the two diagrams (see Sec. III A).
- ⁵⁷ Notice that the fact that the second term is the half-sum of the other two is the result of the particle-hole symmetry in the Hubbard model at half-filling. If it is violated, as may be the case in real materials, then, strictly speaking, a triple resonance would not occur. We will assume that the violation of particle-hole symmetry can be neglected.
- ⁵⁸ This is even more true in the case of polar materials, since the Frohlich electron-phonon interaction, which is singular at the minimum of the fermionic band, precludes large

electron momentum changes, further confining the electronic states to the vicinity of the critical point.

⁵⁹ R. M. Martin, Phys. Rev. B **10**, 2620 (1974).

⁶⁰ Actually, for $\lambda_i < 9/4$, there exists a second solution for $q_x = 0$, but this solution is located well inside the shaded region in Fig 10 and is therefore irrelevant to our considerations.

⁶¹ F. Nori, E. Gagliano, and S. Bacci, Phys. Rev. Lett. **68**, 240 (1992); S. Bacci, E. Gagliano, and F. Nori, Int. J. Mod. Phys. B **5**, 325 (1991); S. Bacci and E. Gagliano, Phys. Rev. B **43**, 6224 (1991).

⁶² R. Liu, private communication.

⁶³ M. V. Klein, in *Dynamical Properties of Solids*, G. K. Horton and A. A. Maradudin, eds. (Elsevier Science Publishers B. V., 1990).

⁶⁴ J. P. Falck, A. Levy, M. A. Kastner and R. J. Birgeneau, Phys. Rev. Lett. **69**, 1109 (1992).

⁶⁵ G. Blumberg, M. V. Klein, private communication (to be published).

⁶⁶ G. Blumberg, private communication.

⁶⁷ W. H. Weber and G. W. Ford, Phys. Rev. B **40**, 6890 (1989).

⁶⁸ S. Rosenblum, A. H. Francis, and R. Merlin, Univ. of Michigan, Ann Arbor, preprint (1993).

⁶⁹ D. V. Khveshchenko and P. B. Wiegmann, Phys. Rev. Lett **73**, 500 (1994).

FIGURES

FIG. 1. A typical Raman cross-section as a function of transferred photon frequency. A two-magnon peak is clearly seen. Data courtesy of the authors of Ref. 18.

FIG. 2. The strength of the two-magnon peak as a function of incoming photon frequency. Also shown is the imaginary part of the dielectric constant. Data courtesy of the authors of Ref. 18. The data in the Figure were obtained at room temperatures. At low T , both the peak in the optical absorption and the Raman profile shift to higher frequencies by about $0.1eV$.^{64,65} The position of the peak in *YBCO* has been reexamined in recent studies⁶⁵, which place the maximum at $\omega_i \sim 3 eV$ rather than $2.8eV$, as in the figure.

FIG. 3. The real-space picture of the two-magnon scattering. Dashed lines denote photons, and wavy lines denote spin waves. The explanations are given in the text. This picture is valid away from resonance.

FIG. 4. The diagrams for two-magnon emission which contribute to the Loudon-Fleury Hamiltonian at small incident frequencies. Each fermion can belong to either the valence (dashed line) or conduction (solid line) band. The emitted magnons are denoted by the solid wavy lines, and the incoming (ω_i) and outgoing (ω_f) photons by the dash-dotted lines at the ends of the diagrams. Additional graphs are obtained from each diagram by the fermion flow reversal and/or flipping all the spin labels.

FIG. 5. Additional graphs which are of the same order of magnitude in t/U as those of Fig. 3, but have extra smallness in $1/S$. The four-fermion vertex is the Hubbard interaction term U . Graph (a) is obtained from Fig. 3(c) by the insertion of a particle-hole bubble in place of a single four-fermion interaction. A sequence of such bubbles sums up to an internal magnon line; an example is given in (b).

FIG. 6. A series of diagrams with the final-state magnon-magnon interactions. The black dot is the Loudon-Fleury vertex for the photon-magnon interaction.

FIG. 7. The profile of the scattering cross-section in the B_{1g} geometry without the final-state magnon-magnon interactions (dashed line) and with final-state interaction (solid and dotted line). The solid and dashed lines were obtained, correspondingly, by using the full expression for $I(\omega)$ in (refI) and its expansion near the top of magnon band which is in line with $1/S$ expansion. Notice that while the position of the two-magnon peak is the same in both cases, the expansion near the top of magnon band yields much broader two-magnon peak.

FIG. 8. Diagrams which become important at resonance. All three denominators in the diagram (a) can vanish simultaneously which is known as a triple resonance. This diagram is dominant in the resonance region. Additional relevant diagrams are generated by the spin label reversal (in both (a) and (b)) and/or the emission of two magnons from the valence band fermion line (in the diagram (b)).

FIG. 9. The lowest order vertex (a) and self-energy (b) corrections to the mean-field theory.

FIG. 10. The triple resonance region (shaded) in the $(\lambda_i, (\omega_i - \omega_f)/4JS)$ plane where $\lambda_i = (\omega_i - 2\Delta)/4JS$. Dashed line - solution for a triple resonance for magnon momentum $q_x = q_y$; solid line - solution for $q_x = 0$ or $q_y = 0$. The horizontal line corresponds to the position of the two-magnon peak at $(\omega_i - \omega_f)/4JS = 2\bar{\omega} = 1.4$.

FIG. 11. (a) The plot of Eq. (22) for the optical conductivity, in the limit $t \ll U$. It has a square root divergence at the lower band edge, and vanishes at the upper band edge. The divergence will be washed out in practice, but we can still expect most prominent features to be located towards the bottom of the SDW quasiparticle band. (b) A schematic illustration of the relative location of the strongest Raman and optical features as a function of the incident photon frequency. Their relative position is a key result of this work. The two solid lines represent the fermion dispersion curves in the conduction and valence bands.

FIG. 12. A fit of the experimental dependence of the inverse two-magnon peak intensity in $YB_2Cu_3O_6$ from Fig. 2 to the theoretical $1/(\omega_i^{res} - \omega_i)$ dependence, Eq. (70). The value of ω_i^{res} from the fit is $\approx 3.1eV$.

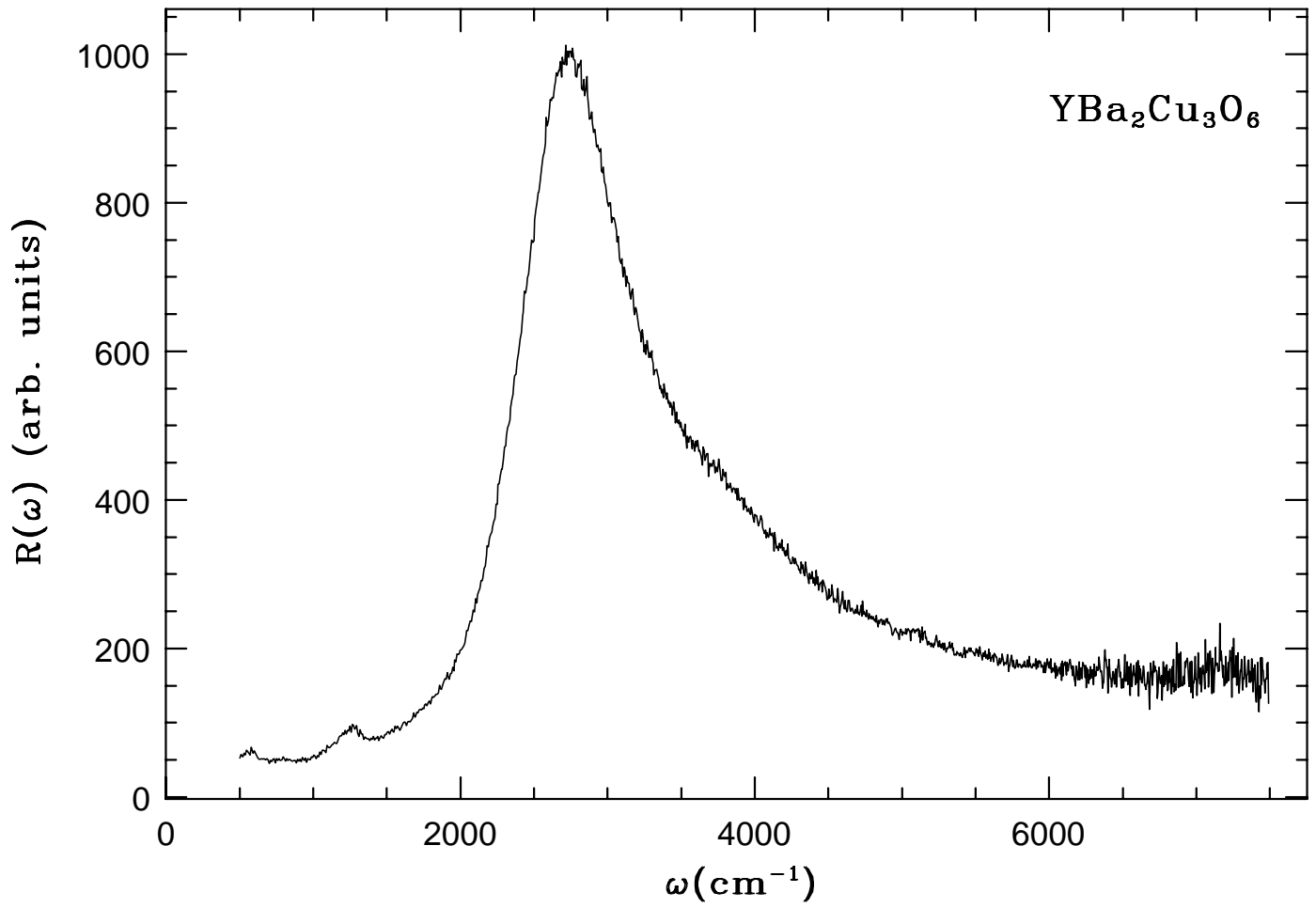


Fig. 1

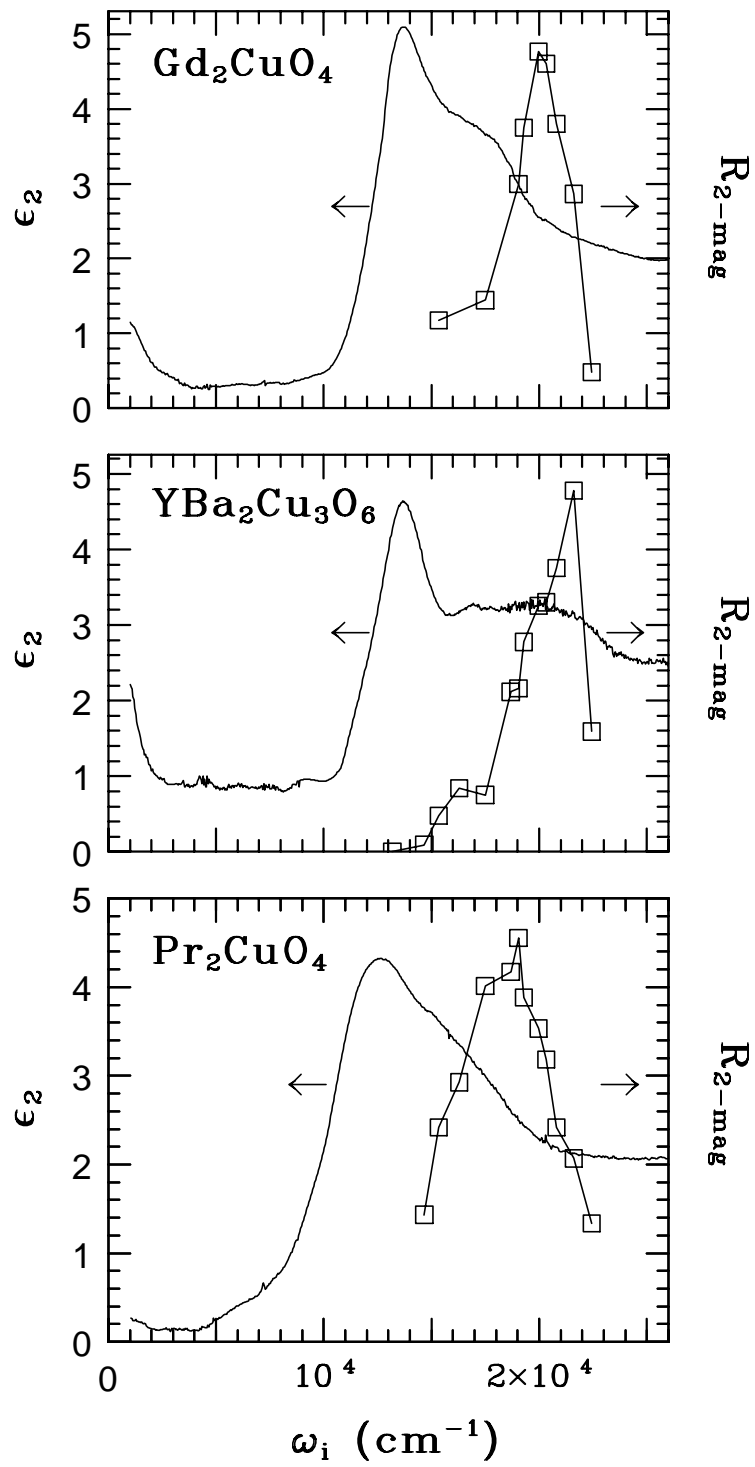


Fig. 2

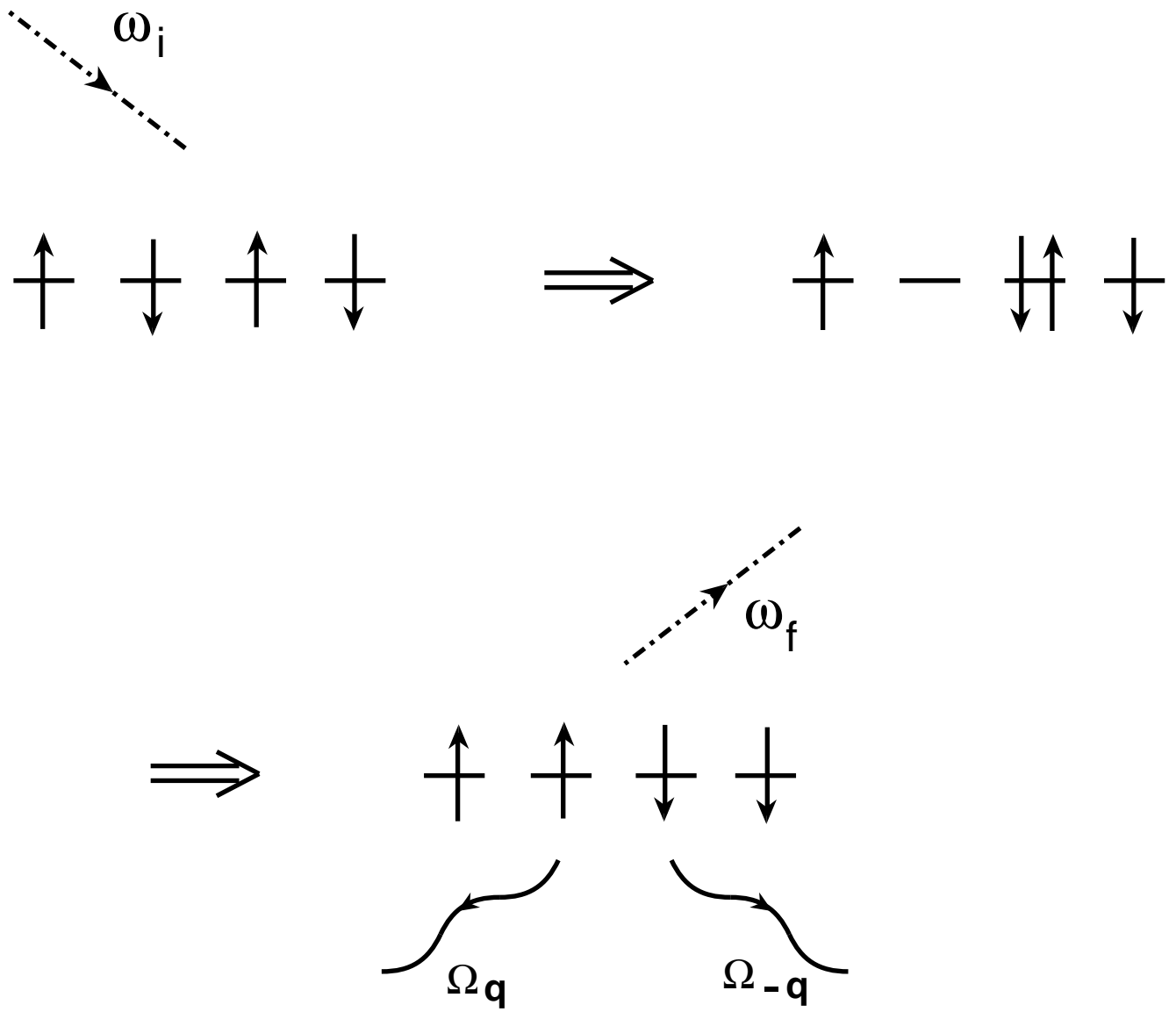
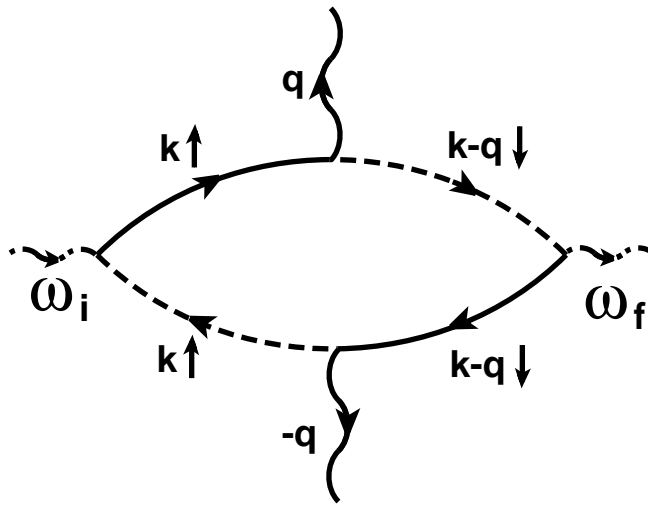
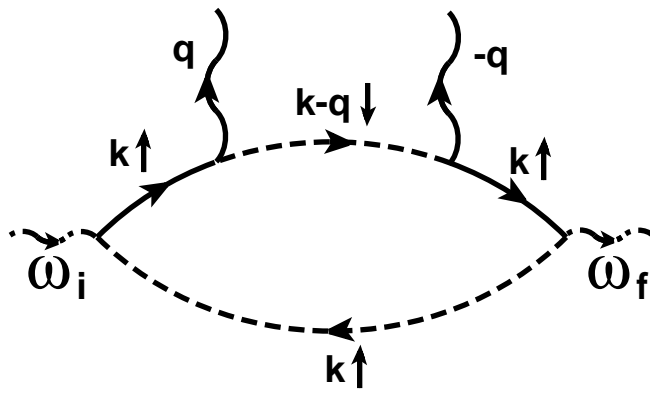


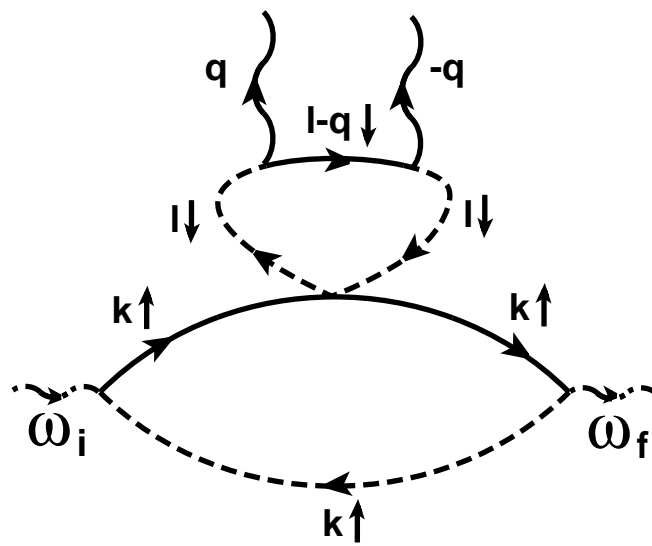
Fig. 3



(a)

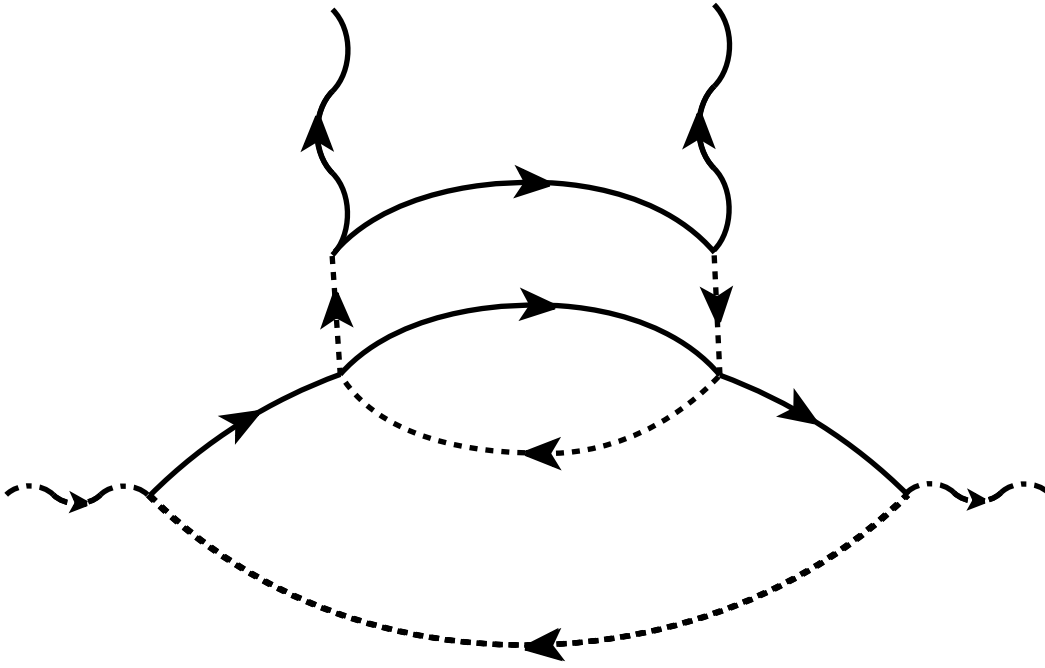


(b)

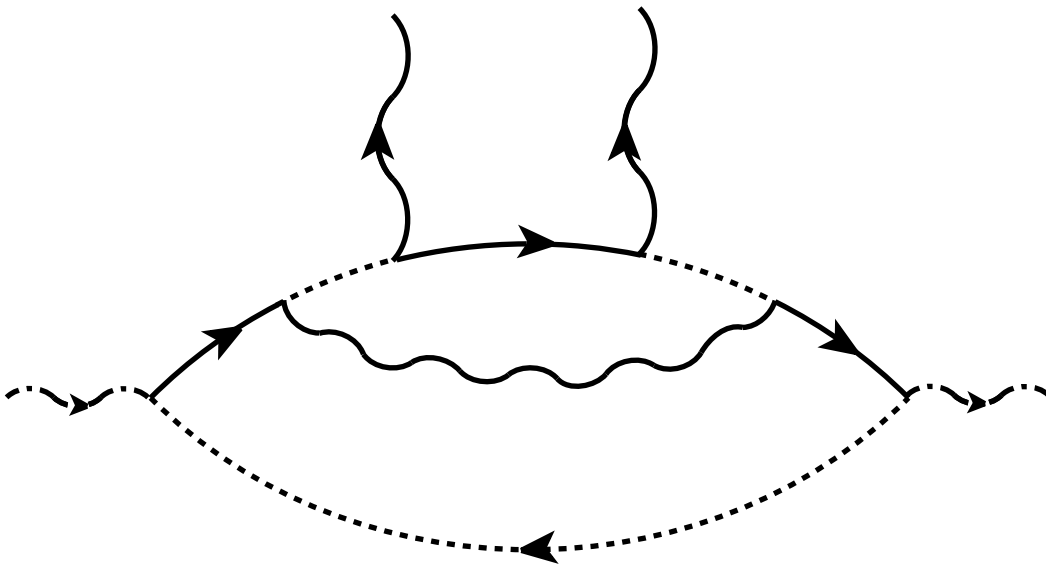


(c)

Fig. 4



(a)



(b)

Fig. 5

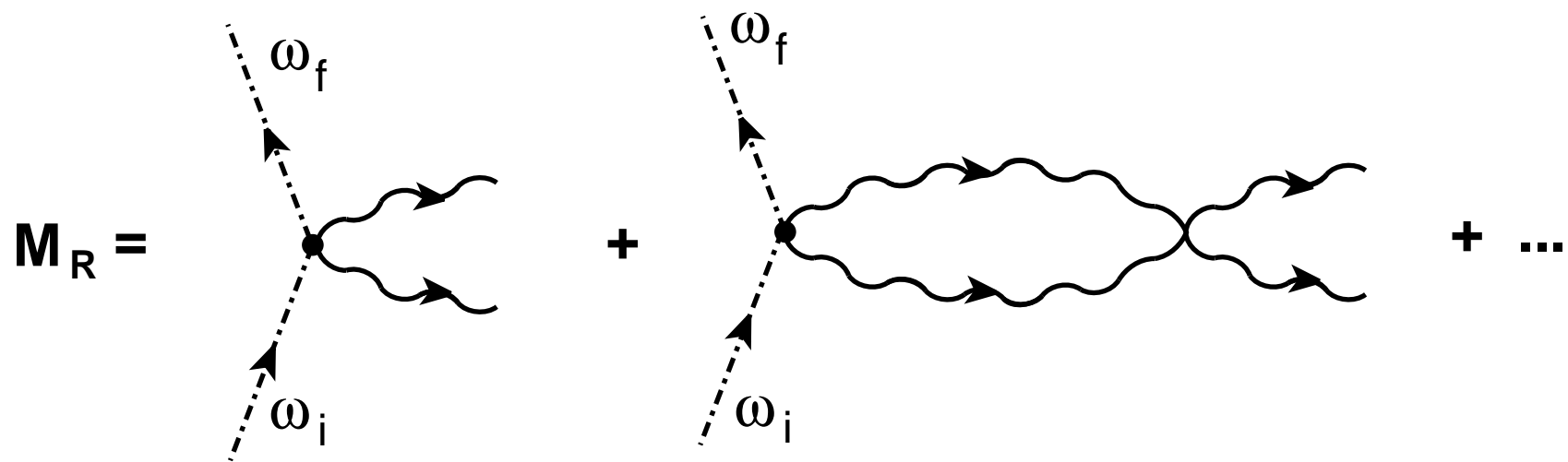


Fig. 6

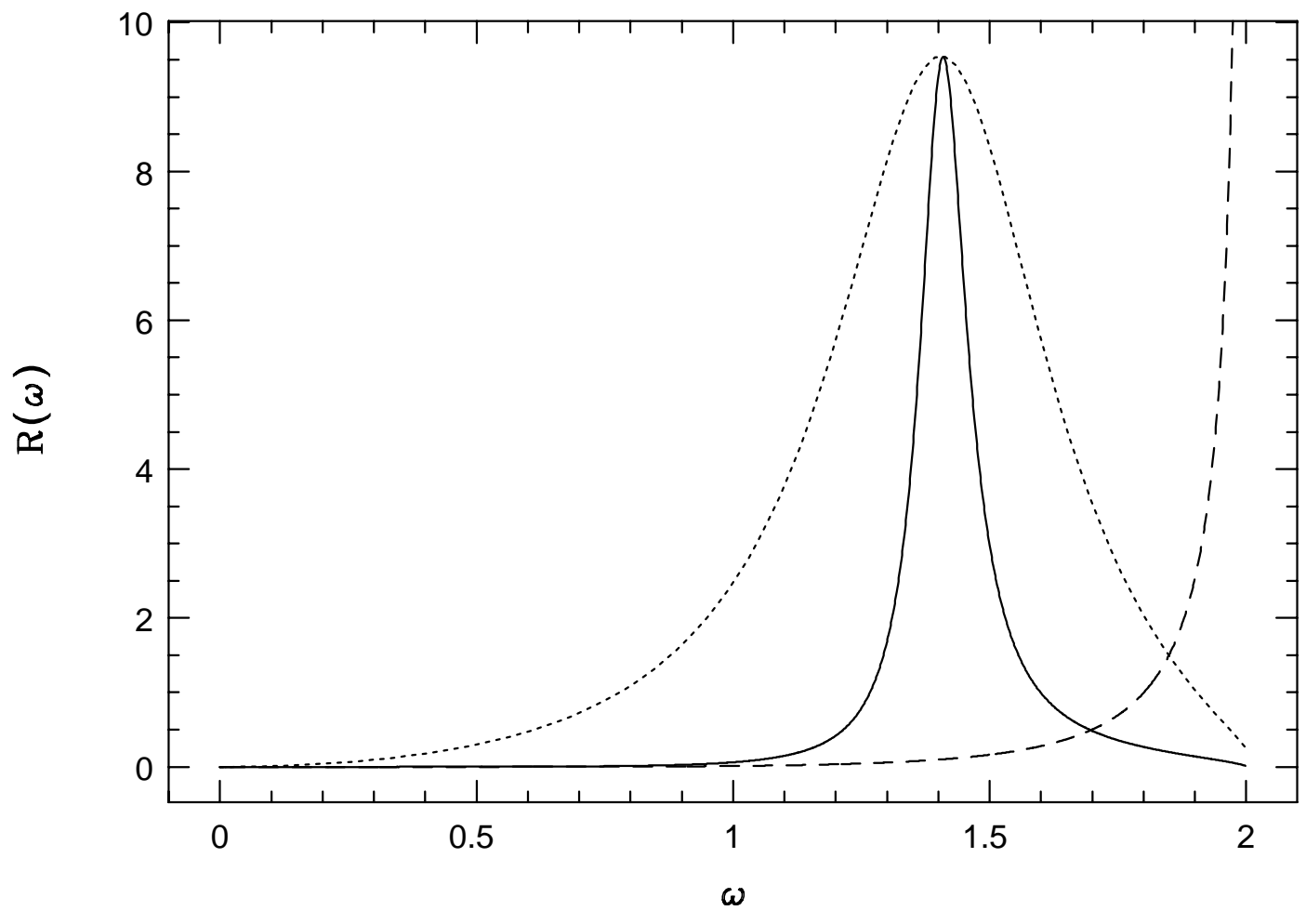
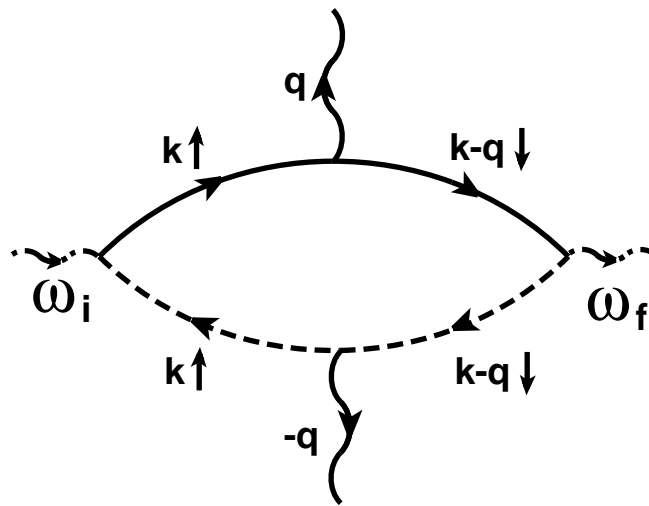
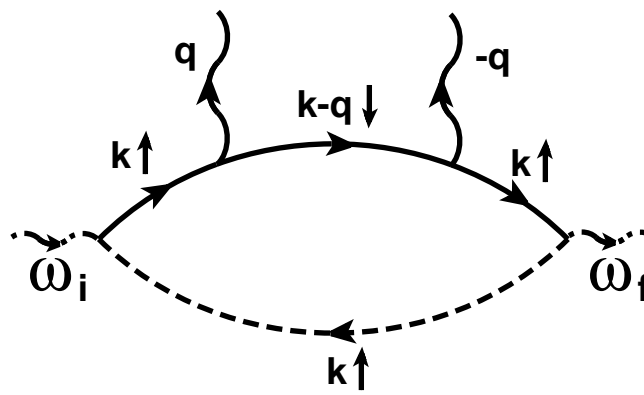


Fig. 7

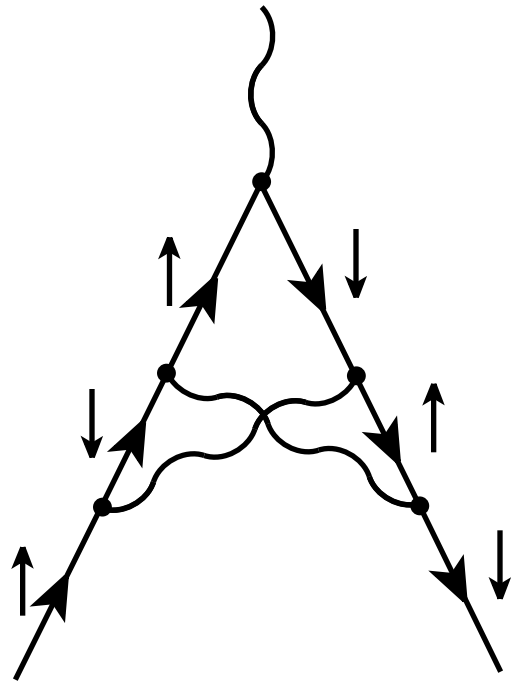


(a)

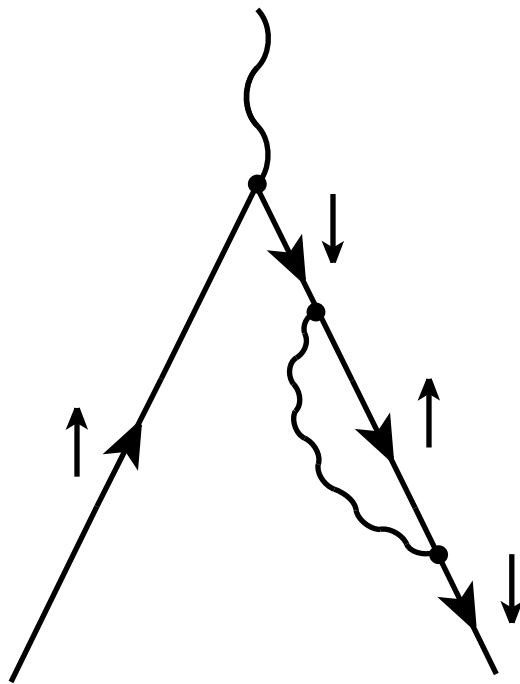


(b)

Fig. 8



(a)



(b)

Fig. 9

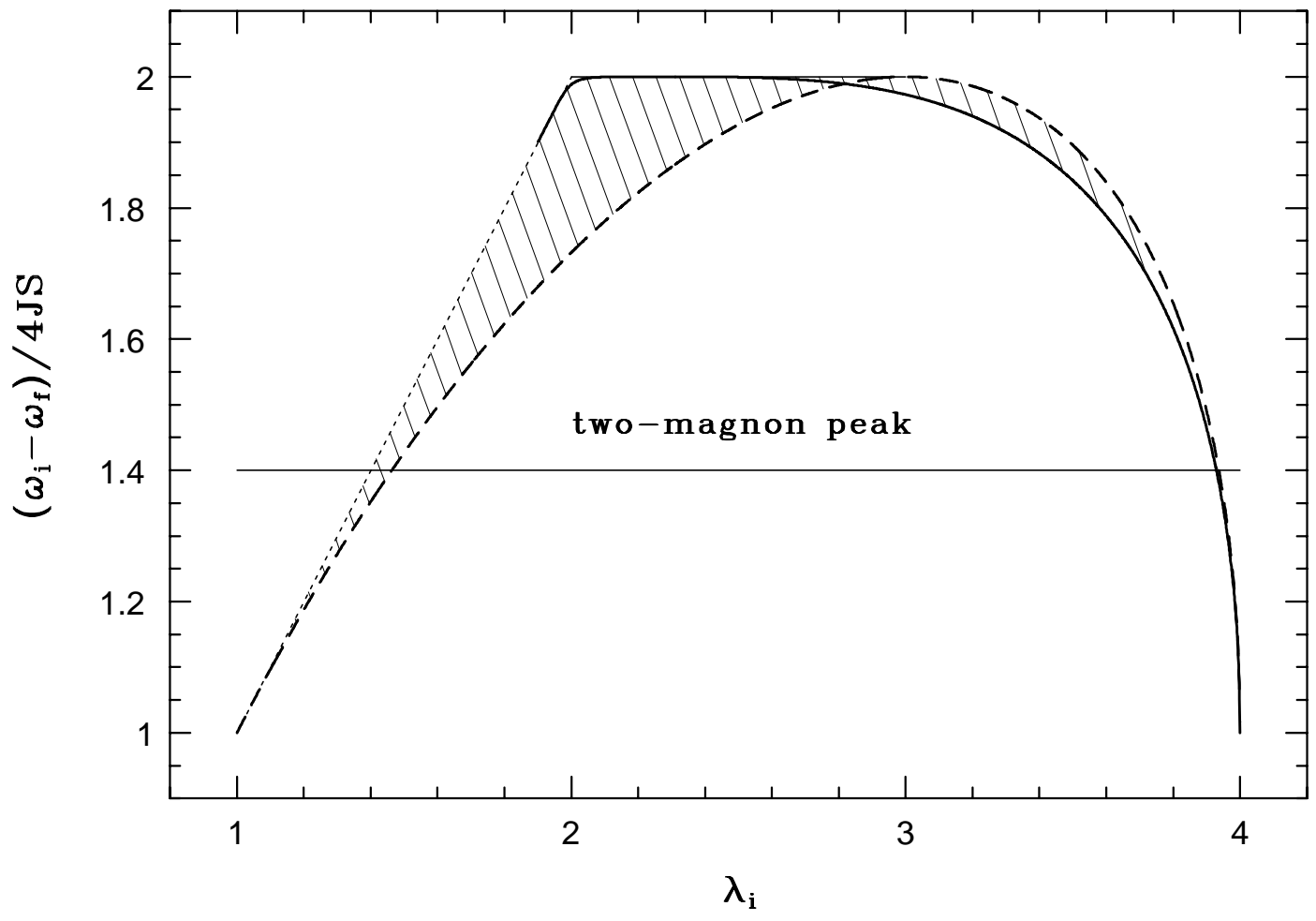
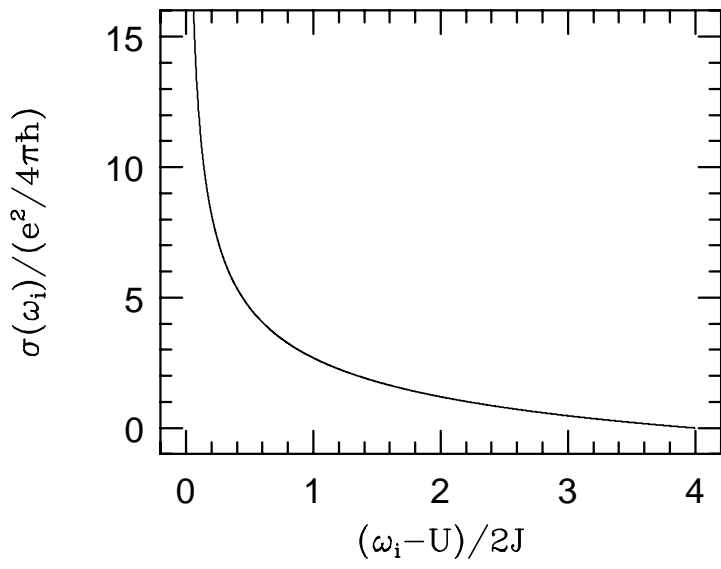
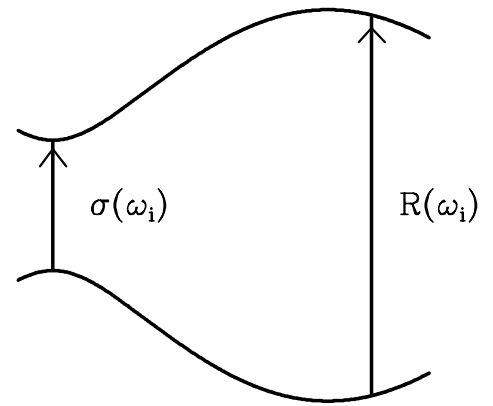


Fig. 10



(a)



(b)

Fig. 11

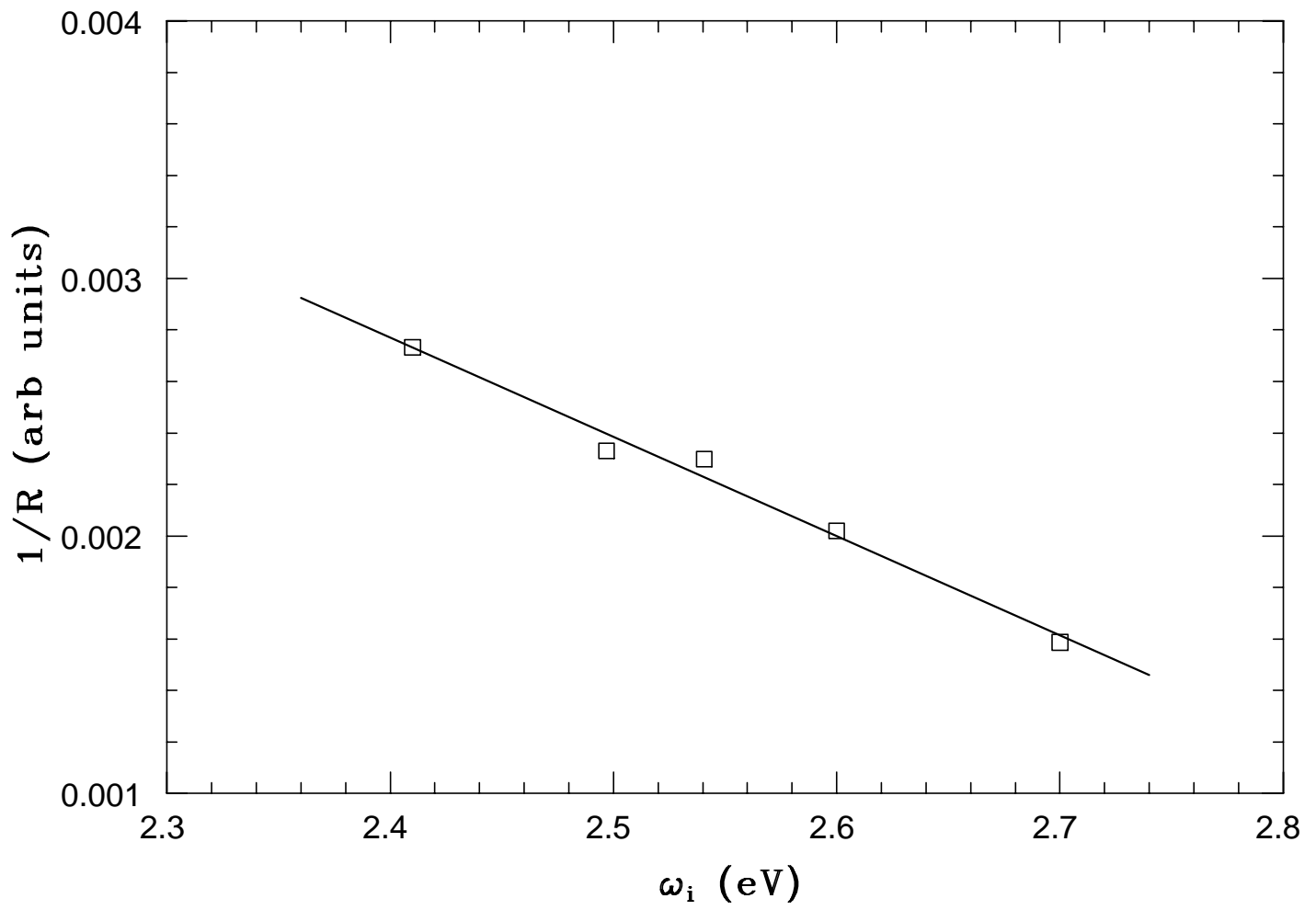


Fig. 12